

1 **Biogenic volatile organic compound ambient mixing ratios and emission rates** 2 **in the Alaskan Arctic tundra**

3 **Hélène Angot¹, Katelyn McErlean¹, Lu Hu², Dylan B. Millet³, Jacques Hueber¹, Kaixin Cui¹, Jacob Moss¹,**
4 **Catherine Wielgasz², Tyler Milligan¹, Damien Ketcherside², M. Sydonia Bret-Harte⁴, Detlev Helmig¹**

5 ¹Institute of Arctic and Alpine Research, University of Colorado Boulder, Boulder, CO, USA.

6 ²Department of Chemistry and Biochemistry, University of Montana, Missoula, MT, USA.

7 ³Department of Soil, Water, and Climate, University of Minnesota, Minneapolis-Saint Paul, MN, USA.

8 ⁴Institute of Arctic Biology, University of Alaska-Fairbanks, Fairbanks, Alaska, USA.

9

10 **Abstract**

11 Rapid Arctic warming, a lengthening growing season, and increasing abundance of biogenic volatile
12 organic compounds (BVOC)-emitting shrubs are all anticipated to increase atmospheric BVOCs in the
13 Arctic atmosphere, with implications for atmospheric oxidation processes and climate feedbacks.
14 Quantifying these changes requires an accurate understanding of the underlying processes driving BVOC
15 emissions in the Arctic. While boreal ecosystems have been widely studied, little attention has been paid to
16 Arctic tundra environments. Here, we report terpenoid (isoprene, monoterpenes, and sesquiterpenes)
17 ambient mixing ratios and emission rates from key dominant vegetation species at Toolik Field Station
18 (TFS; 68°38'N, 149°36'W) in northern Alaska during two back-to-back field campaigns (summers 2018
19 and 2019) covering the entire growing season. Isoprene ambient mixing ratios observed at TFS fell within
20 the range of values reported in the Eurasian taiga (0-500 pptv), while monoterpene and sesquiterpene
21 ambient mixing ratios were respectively close to and below the instrumental quantification limit (~2 pptv).
22 Isoprene surface emission rates ranged from 0.2 to 2250 $\mu\text{gC}/\text{m}^2/\text{h}$ (mean of 85 $\mu\text{gC}/\text{m}^2/\text{h}$) and monoterpene
23 emission rates remained on average below 1 $\mu\text{gC}/\text{m}^2/\text{h}$ over the course of the study. We further quantified
24 the temperature dependence of isoprene emissions from local vegetation including *Salix* spp. (a known
25 isoprene emitter), and compared the results to predictions from the Model of Emissions of Gases and
26 Aerosols from Nature version 2.1 (MEGAN2.1). Our observations suggest a 180-215% emission increase
27 in response to a 3-4°C warming and the MEGAN2.1 temperature algorithm exhibits a close fit with
28 observations for enclosure temperatures in the 0-30°C range. The data presented here provide a baseline to
29 investigate future changes in the BVOC emission potential of the under-studied Arctic tundra environment.

30 **1. Introduction**

31 As a major source of reactive carbon to the atmosphere, biogenic volatile organic compounds
32 (BVOCs) emitted from vegetation play a significant role in global carbon and oxidation cycles
33 (Fehsenfeld et al., 1992). Global emission estimates of BVOCs are in the range of 700-1100 TgC
34 per year, ~70-80% of which corresponds to terpenoid species: isoprene, monoterpenes (MT), and
35 sesquiterpenes (SQT) (Guenther et al., 1995, 2006; Sindelarova et al., 2014). Despite their
36 relatively short atmospheric lifetimes (a few minutes to 1 day for terpenoids), BVOCs affect
37 climate through their effects on the hydroxyl radical (OH, which dictates the lifetime of
38 atmospheric methane), tropospheric ozone (O₃, a key greenhouse gas), and aerosols (which
39 influence radiative scattering) (Arneth et al., 2010; Fuentes et al., 2000; Peñuelas and Staudt,
40 2010). The oxidation of those BVOCs also drives the formation of secondary organic aerosols
41 (SOA) through both gas- and aqueous-phase mechanisms (Carlton et al., 2009; Lim et al., 2005).
42 The potential for increased SOA formation, expected to result in climate cooling (Kulmala et al.,
43 2004), complicates the climate feedbacks of BVOC emissions (Tsigaridis and Kanakidou, 2007;
44 Unger, 2014).

45 Global models of BVOC emissions assume minimal emissions from the Arctic due to low leaf
46 area index and relatively cold temperatures (Guenther et al., 2006; Sindelarova et al., 2014).
47 However, this assumption relies on few observations and has been increasingly challenged by field
48 data (Tang et al., 2016). Recent measurements have revealed significant BVOC emissions from
49 Arctic tundra and vegetation, including *Sphagnum* mosses, wetland sedges, and dwarf shrubs
50 (Ekberg et al., 2009, 2011; Faubert et al., 2010; Holst et al., 2010; Lindfors et al., 2000; Potosnak
51 et al., 2013; Rinnan et al., 2011; Schollert et al., 2014; Tiiva et al., 2008). These results are of
52 importance because BVOC emissions are expected to increase in the Arctic due to climate
53 warming and associated vegetation and land cover change (Faubert et al., 2010; Potosnak et al.,
54 2013; Rinnan et al., 2011; Tiiva et al., 2008). Field warming studies have shown strong increases
55 in BVOC emissions from shrub heath (Michelsen et al., 2012; Tiiva et al., 2008). Furthermore, the
56 temperature dependence of Arctic BVOC fluxes appears to be significantly greater than for tropical
57 and subtropical ecosystems (Holst et al., 2010; Rinnan et al., 2014), with up to 2-fold increases in
58 MT emissions and 5-fold increases in SQT emissions by subarctic heath for a 2°C warming
59 (Valolahti et al., 2015). Similarly, Kramshøj et al. (2016) and Lindwall et al. (2016) examined the

60 response of BVOC emissions to an experimental 3-4°C warming and reported a 260-280%
61 increase in total emissions. Together, the above results emphasize the strong temperature
62 sensitivity of BVOC emissions from Arctic ecosystems.

63 Changing BVOC emissions in the Arctic due to climate and land cover shifts can thus be expected
64 to perturb the overall oxidative chemistry of the region. Previous studies have hypothesized that
65 BVOCs might already impact the diurnal cycle of ozone in the Arctic boundary layer (Van Dam
66 et al., 2016). Changing BVOC emissions can also further affect climate through various feedback
67 mechanisms; Quantifying these changes requires an accurate understanding of the underlying
68 processes driving BVOC emissions in the Arctic. While BVOC ambient mixing ratios and
69 emission rates have been studied in boreal ecosystems, less attention has been paid to Arctic tundra
70 environments (Lindwall et al., 2015). Here, we report BVOC ambient mixing ratios and emission
71 rates at Toolik Field Station (TFS) in the Alaskan Arctic. This study builds on the previous
72 isoprene study at TFS by Potosnak et al. (2013), while also providing a major step forward from
73 that work. In particular, we present the first continuous summertime record of ambient BVOCs
74 (including isoprene and MT) and their first-generation oxidation products in the Arctic tundra
75 environment. The data presented here provide a baseline to investigate future changes in the BVOC
76 emission potential of the under-studied Arctic tundra environment. Due to increasing shrub
77 prevalence across northern Alaska (Berner et al., 2018; Tape et al., 2006), as well as the Eurasian
78 (Macias-Fauria et al., 2012) and Russian Arctic (Forbes et al., 2010), the results of this study have
79 significance to tundra ecosystems across a vast region of the Arctic. We further compare the
80 observed temperature dependence of isoprene emissions with predictions from the Model of
81 Emissions of Gases and Aerosols from Nature version 2.1 (MEGAN2.1), a widely used modeling
82 framework for estimating ecosystem-atmosphere BVOC fluxes (Guenther et al., 2012).

83 **2. Material and Methods**

84 **2.1 Study site**

85 This study was carried out at TFS, a Long-Term Ecological Research (LTER) site located in the
86 tundra on the north flank of the Brooks Range in northern Alaska (68°38'N, 149°36'W; see Fig.1).
87 Vegetation speciation and dynamics, and their changes over time, have been well documented at
88 the site. *Betula* (birch) and *Salix* (willow) are the most common deciduous shrubs (Kade et al.,
89 2012). Common plant species include *Betula nana* (dwarf birch), a major player in ongoing Arctic

90 greening (Hollesen et al., 2015; Sistla et al., 2013), *Rhododendron tomentosum* (formerly *Ledum*
91 *palustre*; Labrador tea); *Vaccinium vitis-idaea* (lowbush cranberry), *Eriophorum vaginatum*
92 (cotton grass), *Sphagnum angustifolium* (peat moss), *Alectoria ochroleuca* (witches hair lichen),
93 and many other perennial species of *Carex*, mosses, and lichens. Vegetation cover at this site is
94 classified as tussock tundra (see Fig.1), which is the most common vegetation type in the northern
95 foothills of the Brooks Range (Elmendorf et al., 2012; Kade et al., 2012; Shaver and Chapin, 1991;
96 Survey, 2012; Walker et al., 1994).

97 Emission measurements and atmospheric sampling were conducted from a weatherproof
98 instrument shelter located ~350 m to the west of TFS (see Fig.S.I.1). Winds at TFS are
99 predominantly from the southerly and northerly sectors (Toolik Field Station Environmental Data
100 Center, 2019), minimizing any influence from camp emissions at the site. Two field campaigns
101 were carried out: the first from mid-July to mid-August 2018, and the second from mid-May to
102 the end of June 2019. These two back-to-back campaigns cover the entire growing season (Sullivan
103 et al., 2007), from the onset of snow melt mid-May to the first snow fall mid-August.

104 **2.2 Ambient online measurements of BVOCs and their oxidation products**

105 2.2.1 Gas chromatography and mass spectrometry with flame ionization detector 106 (GC-MS/FID)

107 An automated GC-MS/FID system was deployed for continuous measurements of atmospheric
108 BVOCs at ~2-hour time resolution during the 2018 and 2019 field campaigns. In addition, the
109 system was operated remotely following the 2018 campaign (through September 15th) to collect
110 background values at the beginning of autumn. Air was pulled continuously from an inlet on a 4
111 m meteorological tower located approximately 30 m from the instrument shelter (Van Dam et al.,
112 2013). Air passed through a sodium thiosulfate-coated O₃ scrubber for selective O₃ removal – to
113 prevent sampling losses and artifacts for reactive BVOCs (Helmig, 1997; Pollmann et al., 2005) –
114 and through a moisture trap to dry the air to a dew point of -45°C. The moisture trap was a U-
115 shaped SilcoSteel™ tube (stainless steel treated) cooled using thermoelectric coolers. Analytes
116 were concentrated on a Peltier-cooled (-40°C) multistage micro-adsorbent trap (50 % Tenax-GR
117 and 50 % Carboxen 1016). Analysis was accomplished by thermal desorption and injection for
118 cryogen free GC using a DB-1 column (60 m × 320 μm × 5 μm) and helium as carrier gas. The
119 oven temperature was set to 40°C for 6 minutes, then increased to 260°C at 20°C/min, and held

120 isothermally at 260°C for 13 minutes. The column flow was split between an FID and a MS for
121 simultaneous quantification and identification. Blanks and calibration standards were regularly
122 injected from a manifold. Isoprene (m/z 67 and 68), methacrolein (MACR) and methylvinylketone
123 (MVK) (m/z 41, 55, and 70), MT (m/z 68, 93, 121, and 136), and SQT (m/z 204, 91, 93, 119, and
124 69) were identified and quantified using the MS in selected ion-monitoring mode (SIM). The
125 response to isoprene was calibrated using a primary gas standard supplied by the National Physical
126 Laboratory (NPL), certified as containing 4.01 ± 0.09 ppb of isoprene in a nitrogen matrix. The
127 analytical uncertainty for isoprene was estimated at 16 % based on the certified uncertainty of the
128 standard and on the repeatability of standard analysis throughout the campaigns. Instrument
129 responses for MACR, MVK, α -pinene, and acetonitrile were calibrated with multi-component
130 standards containing 1007 ppb MACR, 971 ppb MVK, 967 ppb α -pinene, and 1016 ppb
131 acetonitrile (Apel-Riemer Environmental Inc., Miami, FL, USA) dynamically diluted into a stream
132 of ultra-zero grade air to ~ 3 ppb. Quantification of other terpenoid compounds was based on GC
133 peak area (FID response) plus relative response factors using the effective carbon number concept
134 (Faiola et al., 2012; Scanlon and Willis, 1985). The limit of quantification (LOQ) was ~ 2 pptv
135 (pmol/mol by volume). In order to monitor and correct for long-term trends in the detection system,
136 including detector drift and decreasing performance of the adsorbent trap, we used peak areas for
137 long-lived chlorofluorocarbons (CFCs) that were monitored in the air samples together with the
138 BVOCs as an internal reference standard. The atmospheric trace gases CCl_3F (CFC-11) and
139 $\text{CCl}_2\text{FCCl}_2\text{F}_2$ (CFC-113) are ideal in this regard because they are ubiquitous in the atmosphere and
140 exhibit little spatial and temporal variability (Karbiwnyk et al., 2003; Wang et al., 2000).

141 2.2.2 Proton-Transfer-Reaction Time-of-Flight Mass-Spectrometry (PTR-ToF-MS)

142 During the summer 2019 campaign, isoprene mixing ratios in ambient air were also measured by
143 PTR-ToF-MS (model 4000, Ionicon Analytik GmbH, Innsbruck, Austria). The sample inlet was
144 located on the 4 m meteorological tower, right next to the GC-MS/FID inlet. In brief, ambient air
145 was continuously pulled through the PTR-ToF-MS drift-tube, where VOCs with proton affinities
146 higher than that of water (>165.2 kcal/mol) were ionized via proton-transfer reaction with primary
147 H_3O^+ ions, then subsequently separated and detected by a time-of-flight mass spectrometer (with
148 a mass resolving power up to 4000). At TFS, the PTR-ToF-MS measured ions from 17–400 m/z
149 every 2 minutes. Ambient air was drawn to the instrument at 10–15 L/min via ~ 30 m of 1/4" O.D.

150 PFA tubing maintained at $\sim 55^{\circ}\text{C}$, and then subsampled by the instrument through ~ 100 cm of
151 $1/16''$ O.D. PEEK tubing maintained at 60°C . The residence time from the inlet on the 4 m
152 meteorological tower to the drift-tube was less than 5 seconds. Instrument backgrounds were
153 quantified approximately every 5 hours for 20 minutes during the campaign by measuring VOC-
154 free air generated by passing ambient air through a heated catalytic converter (375°C , platinum
155 bead, 1 % wt. Pt, Sigma Aldrich). Calibrations were typically performed every 4 days via dynamic
156 dilution of certified gas standard mixtures containing 25 distinct VOCs including isoprene (Apel-
157 Riemer Environmental Inc., Miami, FL, USA). Here, we report isoprene mixing ratios to inter-
158 compare with GC-MS measurements; other species will be reported in future work. The
159 measurement uncertainty for isoprene is $\sim 25\%$, which includes uncertainties in the gas standards,
160 calibration method, and data processing.

161 2.2.3 Instrument inter-comparison

162 Figure S.I.2 shows a comparison of the GC-MS and PTR-ToF-MS isoprene mixing ratios in
163 ambient air. With a correlation coefficient of 0.93 and a linear regression slope of 0.7-1.0, the two
164 measurements agreed within their combined measurement uncertainties, in line with earlier inter-
165 comparison studies (e.g., Dunne et al., 2018; de Gouw et al., 2003). Similarly, we found a
166 correlation coefficient of 0.96 between GC-MS and PTR-ToF-MS MVK+MACR mixing ratios
167 (not shown). The good agreement between these two independent techniques gives us confidence
168 that the ambient air results presented here are robust.

169 2.3 Ambient air vertical profiles

170 Vertical isoprene mixing ratio profiles were obtained using a 12-foot diameter SkyDoc tethered
171 balloon. A total of eight vertical profiles were performed at ~ 3 -hour intervals between 12:30 pm
172 Alaska Standard Time (AST) on June 15, 2019 and 11:00 am AST on June 16, 2019 in order to
173 capture a full diurnal cycle (solar noon around 2 pm AST). Sampling packages were connected to
174 the tether line such that resulting sampling heights were ~ 30 , ~ 100 , ~ 170 , and ~ 240 m above
175 ground level. One identical sampling package was deployed at the surface. Each sampling package
176 contained an adsorbent cartridge for sample collection (see below) connected to a downstream
177 battery-powered SKC pocket pump controlled using a mechanical relay, a programmable Arduino,
178 and a real-time clock. Once the balloon reached its apex (~ 250 - 300 m a.g.l.), the five pumps were
179 activated simultaneously and samples collected for 30 minutes to ensure that enough material was

180 collected. It should be noted that changes in wind speed and turbulence during the 30-min sampling
181 period often affected the shape of the tethered line and the sampling altitude adding further
182 uncertainty to the vertical profiles presented here. At the end of the 30-min sampling period, the
183 balloon was brought back down. The adsorbent cartridges were prepared in house using glass
184 tubing (89 mm long \times 6.4 mm outer diameter, 4.8 mm inner diameter), and loaded with Tenax-
185 GR and Carboxen 1016 adsorbents (270 mg of each), following established practice (Ortega and
186 Helmig, 2008 and references therein). An inlet ozone scrubber was installed on each cartridge to
187 prevent BVOC sampling losses. Field blanks were collected by opening a cartridge (with no
188 pumped airflow) during each balloon flight. Following collection, adsorbent cartridges were sealed
189 with Teflon-coated brass caps and stored in the dark at $\sim 4^{\circ}\text{C}$ until chemical analysis. Samples were
190 analyzed at the University of Colorado Boulder following the method described in S.I. Section 1.
191 Our previous inter-comparison of this cartridge-GC-MS/FID method with independent and
192 concurrent PTR-MS observations showed that the two measurements agree to within their
193 combined uncertainties at $\sim 25\%$ (Hu et al., 2015). Meteorological conditions were monitored and
194 recorded during each balloon flight with a radiosonde (Met1, Grant Pass, OR, USA) attached to
195 the tethered line just below the balloon.

196 **2.4 BVOC emission rates**

197 **2.4.1 Dynamic enclosure measurements**

198 We used dynamic enclosure systems operated at low residence time to quantify vegetative BVOC
199 emissions following the procedure described by Ortega et al. (2008) and Ortega and Helmig
200 (2008). Two types of enclosures were used: branch and surface chambers. For branch enclosures,
201 a Tedlar® bag (Jensen Inert Products, Coral Springs, FL) was sealed around the trunk side of a
202 branch. For surface enclosures, the bag was placed around a circular Teflon® base (25 cm wide \times
203 16 cm height; see Fig. 2). For both branch and surface enclosures, the bag was connected to a
204 purge-air line and a sampling line, and positioned around the vegetation minimizing contact with
205 foliage. While purging the enclosure (see Section 2.4.3), the vegetation was allowed to acclimate
206 for 24 hours before BVOC sampling began. Samples were collected from the enclosure air,
207 concentrated onto solid-adsorbent cartridges (see Section 2.3) with an automated sampler, and
208 analyzed in-laboratory at the University of Colorado Boulder following the campaign (see S.I.
209 Section 1). Temperature and relative humidity were recorded inside and outside the enclosure (see

210 Fig. 2; S-THB-M002 sensors, Onset HOBO, Bourne, MA, USA) with a data logger (H21-USB,
211 Onset HOBO, Bourne, MA, USA). Additionally, photosynthetically active radiation (400-700 nm;
212 S-LIA-M003, Onset HOBO, Bourne, MA, USA) was measured inside the enclosure. Once
213 installed, enclosures were operated for 2-10 days. The tundra vegetation around TFS is
214 heterogeneous but most dominant species (except *Rubus chamaemorus*) were sampled. Table 1
215 presents the median relative percent cover of plant species in LTER experimental control plots at
216 TFS (Gough, 2019) and indicates whether plant species were present in surface or bag enclosures.
217 The complete list of species sampled and pictures of the enclosures are available in Figures S.I.3-
218 S.I.15; the two sampling sectors are highlighted in Fig.S.I.1. Surface enclosures were divided into
219 three vegetation types: *Salix* spp. (high isoprene emitter), *Betula* spp. (e.g., *Betula nana*
220 dominance), and miscellaneous (mix of different species, including lichens and mosses).

221 2.4.2 Emission rates

222 The emission rate (ER in $\mu\text{gC}/\text{m}^2/\text{h}$) for surface enclosures was calculated as follows:

$$223 \quad ER_{\text{surface}} = \frac{(C_{\text{out}} - C_{\text{in}})Q}{S}, \quad (1)$$

224 where C_{in} and C_{out} are the inlet and outlet analyte concentrations (in $\mu\text{gC}/\text{L}$), Q is the purge air
225 flow rate (in L/h), and S the surface area of the enclosure (in m^2).

226 The ER for branch enclosures (in $\mu\text{gC}/\text{g}/\text{h}$) was calculated as follows:

$$227 \quad ER_{\text{branch}} = \frac{(C_{\text{out}} - C_{\text{in}})Q}{m_{\text{dry}}}, \quad (2)$$

228 where m_{dry} is the dried mass (in g) of leaves enclosed, determined by drying the leaves – harvested
229 after the experiment – at 60-70°C until a consistent weight was achieved (Ortega and Helmig,
230 2008).

231 Emission rates were standardized to 30°C and to a PAR level of 1000 $\mu\text{mol}/\text{m}^2/\text{s}$ using the
232 algorithms described in Guenther et al. (1993, 1995).

233 2.4.3 Enclosure purge air

234 Purge air was provided by an upstream high-capacity oil-free pump providing positive pressure to
235 the enclosure, and equipped with an in-line O_3 scrubber to avoid loss of reactive BVOCs from

236 reaction with O₃ in the enclosure air and during sampling (Helmig, 1997; Pollmann et al., 2005).
237 The purge flow was set to 25 L/min and regularly checked using a volumetric flow meter (Mesa
238 Labs Bios DryCal Defender, Butler, NJ, USA). Excess air escaped from the open end (tied around
239 the Teflon® base) while the sample air flow was pulled into the sampling line (see below).

240 2.4.4 Sample collection

241 A continuous airflow of 400-500 mL/min was drawn from the enclosure through the sampling line.
242 A fraction of this flow was periodically collected at 265-275 mL/min on adsorbent cartridges (see
243 Section 2.3) using a 10-cartridge autosampler (Helmig et al., 2004). During sampling, cartridges
244 were kept at 40°C, *i.e.*, above ambient temperature, to prevent water accumulation on the adsorbent
245 bed (Karbiwnyk et al., 2002). Samples were periodically collected in series to verify lack of analyte
246 breakthrough. Time-integrated samples were collected for 120 min every 2 hours to establish
247 diurnal cycles of BVOC emission. Upon collection, samples were stored in the dark at ~4°C until
248 chemical analysis back at the University of Colorado Boulder.

249 2.4.5 Internal standards

250 In order to identify potential BVOC losses during transport, storage, and chemical analysis, 255
251 of the employed cartridges were pre-loaded with a four-compound standard mixture prior to the
252 field campaigns. These internal standard compounds (toluene, 1, 2, 3-trimethylbenzene, 1, 2, 3, 4-
253 tetrahydronaphtalene, and 1, 3, 5-triisopropylbenzene) were carefully chosen to span a wide range
254 of volatility (C₇-C₁₅) and to not interfere (*i.e.*, coelute) with targeted BVOCs. The recovery of these
255 four compounds was assessed at the end of the campaign, following the analytical procedure
256 described in S.I. Section 1. Recovery rates were 101.8 ± 13.5 % (toluene), 95.2 ± 20.1 % (1,2,3-
257 trimethylbenzene), 95.6 ± 26.6 % (1,2,3,4-tetrahydronaphtalene), and 100.9 ± 18.7 % (1,3,5-
258 triisopropylbenzene). These results indicate that, overall, BVOC losses during transport, storage,
259 and chemical analysis were negligible. Ortega et al. (2008) previously evaluated systematic losses
260 of analytes to enclosure systems similar to those used here. The same four-component standard
261 was introduced into the purge air flow of the enclosures to quantify losses as a function of
262 volatility. That work found median losses of MT and SQT on the order of 20-30%. The emission
263 rates presented here are therefore possibly biased low by a similar amount.

264 2.5 Peak fitting algorithm

265 The analysis of ambient air and enclosure chromatograms was performed using the TERN
266 (Thermal desorption aerosol GC ExploreR and iNtegration package) peak fitting tool implemented
267 in Igor Pro and available online at <https://sites.google.com/site/ternigor/> (Isaacman-VanWertz et
268 al., 2017).

269 **2.6 Ancillary parameters**

270 *Meteorological parameters.* A suite of meteorological instruments was deployed on the 4 m tower.
271 Wind speed and direction were measured at ~4 m above ground level with a Met One 034B-L
272 sensor. As described by Van Dam et al. (2013), temperature was measured at three different heights
273 using RTD temperature probes (model 41342, R.M. Young Company, Traverse City, MI) housed
274 in aspirated radiation shields (model 43502, R.M. Young Company, Traverse City, MI). Regular
275 same-height inter-comparisons were conducted to test for instrumental offsets. Incoming and
276 reflected solar radiation were recorded with LI200X pyranometers (Campbell Scientific
277 Instruments).

278 In addition, historical (1988-2019) meteorological data recorded by TFS Environmental Data
279 Center are available at: https://toolik.alaska.edu/edc/abiotic_monitoring/data_query.php

280 *Particle measurements.* A Met One Instruments Model 212-2 8-channel (0.3 to 10 μm) particle
281 profiler was operated continuously on the roof of the weatherproof instrument shelter. This
282 instrument uses a laser-diode based optical sensor and light scatter technology to detect, size, and
283 count particles (<http://mail.metone.com/particulate-Aero212.htm>).

284 *Nitrogen oxides.* Nitrogen oxides (NO_x) were measured with a custom-built, high sensitivity (~5
285 pptv detection limit) single-channel chemiluminescence analyzer (Fontijn et al., 1970). The
286 instrument monitors nitric oxide (NO) and nitrogen dioxide (NO_2) in ambient air using a photolytic
287 converter. Automated switching valves alternated between NO and NO_2 mode every 30 minutes.
288 Calibration was accomplished by dynamic dilution of a 1.5 ppm compressed NO gas standard
289 (Scott-Marrin, Riverside, CA, USA).

290 **2.7 Theoretical response of isoprene emissions to temperature in MEGAN2.1**

291 We applied our isoprene emission measurements to evaluate the temperature response algorithms
292 embedded in MEGAN2.1 (Guenther et al., 2012). Theoretical isoprene emission rates (F_T) were
293 calculated for TFS as:

$$294 \quad F_T = C_{CE} \gamma_T \sum_j \kappa_j \varepsilon_j \quad (3)$$

295 where C_{CE} is the canopy environment coefficient (assigned a value that results in $\gamma_T = 1$ under
296 standard conditions), and ε_j is the emission factor under standard conditions for vegetation type j
297 with fractional grid box areal coverage κ_j . We used $\sum_j \kappa_j \varepsilon_j = 2766 \mu\text{g}/\text{m}^2/\text{h}$ at TFS based on the
298 high resolution (1 km) global emission factor input file available at
299 <https://bai.ess.uci.edu/megan/data-and-code/megan21>. The temperature activity factor (γ_T) was
300 calculated as:

$$301 \quad \gamma_T = E_{opt} \times \frac{200 e^{95x}}{200 - 95 \times (1 - e^{200x})} \quad (4)$$

302 with

$$303 \quad x = \frac{\frac{1}{T_{opt}} - \frac{1}{T}}{0.00831} \quad (5)$$

$$304 \quad E_{opt} = 2 \times e^{0.08(T_{10} - 297)} \quad (6)$$

$$305 \quad T_{opt} = 313 + 0.6(T_{10} - 297), \quad (7)$$

306 where T is the enclosure ambient air temperature and T_{10} the average enclosure air temperature
307 over the past 10 days.

308 **3. Results and Discussion**

309 **3.1 Ambient air mixing ratios**

310 3.1.1 Isoprene and oxidation products

311 Figure 3 (top panels) shows the time-series of isoprene mixing ratios in ambient air recorded over
312 the course of this study at TFS with the GC system. Mixing ratios were highly variable and ranged
313 from below the quantification limit to 505 pptv (mean of 36.1 pptv). The PTR-ToF-MS gave
314 similar results (see Fig.S.I.16a). These mixing ratios fall within the range of values reported in the
315 Eurasian taiga (e.g., Hakola et al., 2000, 2003; Lappalainen et al., 2009). For example, Hakola et

316 al. (2003) reported a maximum monthly mean mixing ratio of 98 pptv (in July) in Central Finland
317 while Hakola et al. (2000) observed mixing ratios ranging from a few pptv to ~600 pptv in Eastern
318 Finland. In general, however, BVOC emissions in the Eurasian taiga are relatively low compared
319 to forest ecosystems in warmer climates and are dominated by monoterpenes (Rinne et al., 2009).

320 Isoprene mixing ratios peaked on August 1, 2018 around 4 pm and on June 20, 2019 around 10
321 pm, respectively. These two peaks occurred 3-5 hours after the daily maximum ambient
322 temperature was reached (17.8°C in 2018 and 21.8°C in 2019 – see Fig. 3). The isoprene peak on
323 June 20, 2019 was concomitant with enhanced acetonitrile mixing ratios and particle counts (see
324 Fig. 4), reflecting unusually hazy conditions that day at TFS. We attribute the particle and
325 acetonitrile enhancements to intense wildfires occurring across the Arctic Circle at that time – most
326 of them in southern Alaska and Siberia (Earth Observatory, 2019). Acetonitrile increased by a
327 factor of 4 during this event, compared to a factor of 21 increase for isoprene. The higher emission
328 factor for acetonitrile vs. isoprene from biomass burning in boreal forests (Akagi et al., 2011) and
329 the relatively short lifetime of isoprene (Atkinson, 2000) indicate that the observed isoprene
330 enhancement was due to fresh local biogenic emissions rather than transported wildfire emissions.

331 Over the course of this study, we recorded MACR and MVK mixing ratios respectively ranging
332 from below the quantification limit to 95 pptv (12.4 ± 16.1 pptv; mean \pm standard deviation) and
333 from below the quantification limit to 450 pptv (43.1 ± 66.7 pptv; see Fig. 3, top panels). The PTR-
334 ToF-MS gave similar results (see Fig.S.I.16b). Median NO and NO₂ mixing ratios of 21 and 74
335 pptv, respectively, during the 2019 campaign (not shown) suggest a low-NO_x environment, in line
336 with previous studies at several Arctic locations (Bakwin et al., 1992; Honrath and Jaffe, 1992).
337 Under such conditions, MACR and MVK mixing ratios should be used as upper estimates as it has
338 been noted that some low-NO_x isoprene oxidation products (isoprene hydroxyhydroperoxides) can
339 undergo rearrangement in GC and PTR-MS instruments and be misidentified as MACR and MVK
340 (Rivera-Rios et al., 2014). We found a high correlation between MACR and MVK ($R^2 = 0.95$, $p <$
341 0.01) and between these two compounds and isoprene ($R^2 \sim 0.80$, $p < 0.01$). Increases of MACR
342 and MVK mixing ratios above the background were mostly concomitant with isoprene increases,
343 suggesting that atmospheric or within-plant oxidation of isoprene was their main source
344 (Biesenthal et al., 1997; Hakola et al., 2003; Jardine et al., 2012). The mean ratio of MVK to
345 MACR was 2.7, within the range reported by earlier studies (e.g., Apel et al., 2002; Biesenthal and

346 Shepson, 1997; Hakola et al., 2003; Helmig et al., 1998), and no clear diurnal cycle in the ratio
347 was found. This record of ambient air isoprene, MACR, and MVK mixing ratios is, to the best of
348 our knowledge, the first in an Arctic tundra environment. The combined measurement of isoprene
349 and its oxidation products provides a new set of observations to further constrain isoprene
350 chemistry under low-NO_x conditions in atmospheric models (e.g., Bates and Jacob, 2019).

351 3.1.2 Isoprene vertical profiles

352 Figure 5 shows vertical profiles (0 to ~250 m a.g.l.) of isoprene mixing ratios derived from the 30-
353 min tethered balloon samples collected on June 15 and 16, 2019. Temperature profiles (see
354 Fig.S.I.17) indicate that most of the flights were performed in a convective boundary layer (Holton
355 and Hakim, 2013). A nocturnal boundary layer was, however, observed in the first ~50 m from ~2
356 am to ~4:30 am (see Fig.S.I.17e-f) – with temperature increasing with elevation.

357 Except during the last flight, isoprene mixing ratios were in the range of background levels (~0-
358 50 pptv) reported with the GC-MS (see Section 3.1.1). Samples collected from 10-10:30 am on
359 June 16 (see Fig. 5h) showed a pronounced gradient, with 200 pptv at ground level and decreasing
360 mixing ratios with elevation. This maximum at ground-level is expected for a VOC with a surface
361 source (Helmig et al., 1998) while the 200 pptv mixing ratio can likely be attributed to a
362 temperature-driven increase of isoprene emissions by the surrounding vegetation. Indeed, the
363 ambient temperature at ground-level was higher during that flight than during the previous ones
364 (see Fig.S.I.17h). The diurnal cycles of isoprene emissions and temperature are further discussed
365 in Section 3.2.2. Interestingly, the GC-MS and the PTR-ToF-MS did not capture this 200 pptv
366 maximum (see Fig. 3 and Fig.S.I.16), which may be because the balloon flights were performed
367 at a different location (near sampling sector B, see Fig.S.I.1) surrounded by a higher fraction of
368 isoprene-emitting shrubs (willow).

369 Samples collected on June 16, 2019 from 4 to 4:30 am (see Fig. 5f) show decreasing isoprene
370 mixing ratios with increasing elevation, suggesting higher levels (25-50 pptv) in the nocturnal
371 boundary layer than above. This result suggests continuing isoprene emissions by the surrounding
372 vegetation under low-PAR conditions. This is further discussed in Section 3.2.2.

373 3.1.3 Monoterpenes and Sesquiterpenes

374 MT mixing ratios ranged from 3 to 537 pptv (14 ± 18 pptv; median \pm standard deviation) during
375 the 2019 campaign according to the PTR-ToF-MS measurements. Using the GC-MS/FID, we were
376 able to detect and quantify the following MT in ambient air: α -pinene, camphene, sabinene, p-
377 cymene, and limonene. Mean mixing ratios are reported in Table 2 (for values lower than the LOQ,
378 mixing ratios equal to half of the LOQ are used). These compounds have been previously identified
379 as emissions of the widespread circumpolar dwarf birch *Betula nana* (Li et al., 2019; Vedel-
380 Petersen et al., 2015) and other high Arctic vegetation (Schollert et al., 2014). The quantification
381 frequency of camphene, sabinene, p-cymene, and limonene was low (see Table 2) and MT mixing
382 ratios in ambient air were dominated by α -pinene. Several prior studies performed at boreal sites
383 have similarly identified α -pinene as the most abundant monoterpene throughout the growing
384 season (e.g., Hakola et al., 2000; Lindfors et al., 2000; Spirig et al., 2004; Tarvainen et al., 2007).
385 We did not detect any sesquiterpene in ambient air above the 2 pptv instrumental LOQ.

386 Overall, isoprene and α -pinene dominated the ambient air BVOC profile at TFS, respectively
387 constituting $\sim 72\%$ and $\sim 24\%$ of total BVOCs quantified in ambient air (on a mixing-ratio basis).

388 **3.2 Emission rates**

389 3.2.1 Branch enclosures

390 A branch enclosure experiment was performed from July 27 to August 2, 2018 on *Salix glauca* to
391 investigate BVOC emission rates per dry weight plant biomass (see Fig.S.I.5). Isoprene emission
392 rates ranged from <0.01 to $11 \mu\text{gC/g/h}$ (with a mean enclosure temperature of 16.5°C and mean
393 PAR of $880 \mu\text{mol/m}^2/\text{s}$), in line with non-normalized emission rates reported at Kobbefjord,
394 Greenland by Kramshøj et al. (2016; Supplementary Table 5) for the same species under slightly
395 different environmental conditions (mean temperature of 24.6°C and mean PAR of 1052
396 $\mu\text{mol/m}^2/\text{s}$). Once standardized to 30°C and $1000 \mu\text{mol/m}^2/\text{s}$, our emission rates averaged 5
397 $\mu\text{gC/g/h}$, in good agreement with standardized emissions reported at Kobbefjord (mean of 7
398 $\mu\text{gC/g/h}$) by Vedel-Petersen et al. (2015). The quantified MTs had emissions averaging two orders
399 of magnitude lower than those of isoprene (0.01 vs $1 \mu\text{gC/g/h}$). Emission rates for the sum of α -
400 pinene, β -pinene, limonene, camphene, and 1,8-cineole ranged from <0.01 to $0.06 \mu\text{gC/g/h}$. These
401 results are again in good agreement with those reported for the same species at Kobbefjord (~ 0.01
402 $\mu\text{gC/g/h}$) by Kramshøj et al. (2016; Supplementary Table 5).

403 3.2.2 Surface emission rates

404 The isoprene surface emission rate, as inferred from surface enclosures, was highly variable and
405 ranged from 0.2 to ~2250 $\mu\text{gC}/\text{m}^2/\text{h}$ (see Fig. 6). The 2250 $\mu\text{gC}/\text{m}^2/\text{h}$ maximum, reached on June
406 26, 2019, with an enclosure temperature of 32°C, is higher than maximum values reported at TFS
407 by Potosnak et al. (2013) (1200 $\mu\text{gC}/\text{m}^2/\text{h}$ at an air temperature of 22°C). It should be noted that
408 these maximum values were observed at different ambient temperatures; we further investigate the
409 temperature dependency of isoprene emissions in Section 3.3. Elevated surface emission rates (*i.e.*,
410 $> 500 \mu\text{gC}/\text{m}^2/\text{h}$) were all observed while sampling enclosures dominated by *Salix* spp.. At TFS,
411 the overall 24-hour mean isoprene emission rate amounted to 85 $\mu\text{gC}/\text{m}^2/\text{h}$, while the daytime (10
412 am-8 pm) and midday (11 am-2 pm) means were 140 and 213 $\mu\text{gC}/\text{m}^2/\text{h}$, respectively. To put this
413 in perspective, the average isoprene surface emission rate standardized to 30°C and 1000
414 $\mu\text{mol}/\text{m}^2/\text{s}$ ($\sim 300 \mu\text{gC}/\text{m}^2/\text{h}$) was an order of magnitude lower than emission rates reported for
415 warmer mid-latitude or tropical forests. For example, average midday fluxes of 3000 $\mu\text{gC}/\text{m}^2/\text{h}$
416 were reported in a northern hardwood forest in Michigan (Pressley et al., 2005), while several
417 reports of isoprene emissions from tropical ecosystems give daily estimates of 2500-3000
418 $\mu\text{gC}/\text{m}^2/\text{h}$ (Helmig et al., 1998; Karl et al., 2004; Rinne et al., 2002).

419 Figure 7 shows the measured surface emission rates for α -pinene, β -pinene, limonene, and 1,8-
420 cineole. While p-cymene, sabinene, 3-carene, and isocaryophyllene (SQT) were detected in some
421 of the surface enclosure samples, we focus the discussion on the most frequently quantified
422 compounds. It is worth noting that the most frequently observed compounds in enclosure samples
423 are among the most frequently seen MT in ambient air (see Section 3.1.3). Regardless of the
424 species, emission rates remained on average below 1 $\mu\text{gC}/\text{m}^2/\text{h}$ over the course of the study (see
425 Table 3). These results are at the low end of emission rates reported for four vegetation types in
426 high Arctic Greenland (Schollert et al., 2014), but in line with results reported at Kobbefjord,
427 Greenland by Kramshøj et al. (2016; Supplementary Table 4).

428 Figures 8a-c show the mean diurnal cycle (over the two campaigns) of isoprene surface emission
429 rates for different vegetation types (see Fig.S.I.3-15 for nomenclature). The two field campaigns
430 were carried out during the midnight sun period, which could possibly sustain BVOC emissions
431 during nighttime. It should, however, be noted that low sun angles translate to very low PAR and
432 a typical diurnal pattern is observed in summer at TFS despite 24 hours of light (see Fig. 8h).
433 Regardless of the vegetation type, isoprene emission rates exhibited a significant diurnal cycle

434 with an early afternoon maximum, in line with the mean diurnal cycle of enclosure temperature
435 and PAR. These results are in line with the well-established diurnal variation of BVOC emissions
436 in environments ranging from Mediterranean to boreal forests (e.g., Fares et al., 2013; Liu et al.,
437 2004; Ruuskanen et al., 2005; Zini et al., 2001) and with the correlation between isoprene ambient
438 air mixing ratios and temperature at TFS (see Section 3.1). Despite the relatively low MT emission
439 rates, a significant diurnal cycle was also observed with peak total MT emissions of $\sim 1 \mu\text{gC}/\text{m}^2/\text{h}$
440 during early afternoon for both *Salix* spp. and *Betula* spp. (Fig. 8e-f). A summary of emission rates
441 per vegetation type and time of day is given in Table 3. As can be seen in Table 3 and Fig. 8, PAR
442 and BVOC emissions significantly decreased at night but were still detectable. These sustained
443 BVOC emissions during nighttime confirm observations by Lindwall et al. (2015) during a 24-
444 hour experiment with five different Arctic vegetation communities and explain the higher isoprene
445 levels observed in the nocturnal boundary layer than above during the diurnal balloon experiment
446 (see Section 3.1.2).

447 The ratio of total MT (given by the sum of α -pinene, β -pinene, limonene, and 1,8-cineole)
448 emissions to isoprene emissions was an order of magnitude higher for *Betula* spp. (0.22) than for
449 *Salix* spp. (0.03). This result, driven by the relatively lower isoprene emissions of *Betula* spp., is
450 in line with earlier studies, suggesting similar emission characteristics for Arctic plants (e.g.,
451 Kramshøj et al., 2016; Vedel-Petersen et al., 2015).

452 **4. Insights into future changes**

453 **4.1 Response of isoprene emissions to temperature**

454 The Arctic has warmed significantly during the last three decades and temperatures are projected
455 to increase an additional 5-13°C by the end of the century (Overland et al., 2014). Heat wave
456 frequency is also increasing in the terrestrial Arctic (Dobricic et al., 2020). For example, western
457 Siberia experienced an unusually warm May in 2020, with temperatures of 20-25°C (Freedman
458 and Cappucci, 2020). In that context, numerous studies have pointed out the likelihood of increased
459 BVOC emissions due to Arctic warming and associated vegetation and land cover change (Faubert
460 et al., 2010; Potosnak et al., 2013; Rinnan et al., 2011; Tiiva et al., 2008).

461 Over the course of the two field campaigns at TFS, BVOC surface emission rates were measured
462 over a large span of enclosure temperatures (2-41°C). While isoprene and MT emissions respond
463 to leaf temperature (Guenther et al., 1993), air temperature was used here in place of leaf

464 temperature – which has been assumed before in the literature for high-latitude ecosystems (e.g.,
465 Olofsson et al., 2005; Potosnak et al., 2013). Several studies have, however, suggested a
466 decoupling of leaf and air temperature in tundra environments (Lindwall et al., 2016; Potosnak et
467 al., 2013). With predicted increase of air temperature in the Arctic, it still remains largely unknown
468 how leaf temperature will change and impact BVOC emissions. As suggested by Tang et al.
469 (2016), long-term parallel observations of both leaf and air temperature are needed. The response
470 of BVOC emissions to temperature discussed here should be interpreted with this potential caveat
471 in mind.

472 While MT emissions remained low and close to the detection limit thus preventing robust
473 quantification of any emission-temperature relationship, isoprene emissions significantly
474 increased with temperature (Fig.9). Figure 9 combines daytime (e.g., with relatively high PAR
475 values) isoprene emission rates from different surface enclosures, with results normalized to
476 account for differing total biomass and species distributions (with *Salix* spp. the dominant emitter).
477 Specifically, we divided all fluxes by the enclosure-specific mean emission at $20 \pm 1^\circ\text{C}$. Emission
478 rates are often standardized to 30°C but we employ 20°C here owing to the colder growth
479 environment at TFS (Ekberg et al., 2009). The isoprene emission-temperature relationship
480 observed at TFS (in blue) is very similar to that reported by Tang et al. (2016) at Abisko (Sweden;
481 in pink) for tundra heath (dominated by evergreen and deciduous dwarf shrubs). Results at TFS
482 and Abisko both point to a high isoprene-temperature response for Arctic ecosystems (Tang et al.,
483 2016). This is further supported by two warming experiments performed in mesic tundra heath
484 (dominated by *Betula nana*, *Empetrum nigrum*, *Empetrum hermaphroditum*, and *Cassiope*
485 *tetragona*) and dry dwarf-shrub tundra (co-dominated by *Empetrum hermaphroditum* and *Salix*
486 *glauca*) in Western Greenland (Kramshøj et al., 2016; Lindwall et al., 2016). Kramshøj et al.
487 (2016) observed a 240% isoprene emission increase with 3°C warming, while Lindwall et al.
488 (2016) reported a 280% increase with 4°C warming. The observationally-derived emission-
489 temperature relationship derived here for TFS reveals a 180-215% emission increase with 3- 4°C
490 warming.

491 The MEGAN2.1 modeling framework is commonly used to estimate BVOC fluxes between
492 terrestrial ecosystems and the atmosphere (e.g., Millet et al., 2018). Here, we apply the TFS
493 observations to evaluate the MEGAN2.1 emission-temperature relationship for this Arctic

494 environment. Figure 9 shows that the model temperature algorithm provides a close fit with
495 observations below 30°C, with a 170-240% emission increase for a 3-4°C warming. While the
496 model predicts a leveling-off of emissions at approximately 30-35°C, our observations reveal no
497 such phenomenon within the 0-40°C enclosure temperature range (Fig. 9). However, given the
498 limited number of enclosure measurements above 30°C, a leveling-off of emissions cannot be
499 statistically ruled out. The key result here is that MEGAN2.1 adequately reproduces the
500 temperature dependence response of Arctic ecosystems in the 0-30°C temperature range – ambient
501 temperature > 30°C being unlikely. The highest air temperature on record at TFS (1988-2019) is
502 26.5°C, and the mean summertime (June-August) temperature over that period is 9°C.
503 Additionally, for each year in the 1988-2019 historical dataset, there were only 1 to 23 days (0 to
504 4 days) per year with a maximum temperature above 20°C (above 25°C). If global greenhouse gas
505 emissions continue to increase, temperatures are expected to rise 6-7°C in northern Alaska by the
506 end of the century (annual average; Markon et al., 2012) while the number of days with
507 temperatures above 25°C could triple (Lader et al., 2017). Based on current climate conditions and
508 this rate of change, the MEGAN2.1 algorithm adequately represents the temperature dependence
509 response of Arctic ecosystems for the near and intermediate-term future.

510 4.2 Long-term effects of warming

511 BVOC produced by plants are involved in plant growth, reproduction, and defense, and plants use
512 isoprene emissions as a thermotolerance mechanism (Peñuelas and Staudt, 2010; Sasaki et al.,
513 2007). The exponential response of isoprene emissions to temperature observed at TFS adds to a
514 growing body of evidence indicating a high isoprene-temperature response in Arctic ecosystems.
515 However, observations at TFS do not necessarily reflect long-term effects of warming. Schollert
516 et al., (2015) examined how long-term warming affects leaf anatomy of individual arctic plant
517 shoots (*Betula nana*, *Cassiope tetragona*, *Empetrum hermaphroditum*, and *Salix arctica*). They
518 found that long-term warming results in significantly thicker leaves suggesting anatomical
519 acclimation. While the authors hypothesized that this anatomical acclimation may limit the
520 increase of BVOC emissions at plant shoot-level, Kramshøj et al. (2016) later showed that BVOC
521 emissions from Arctic tundra exposed to six years of experimental warming increase at both the
522 plant shoot and ecosystem levels.

523 In addition to the direct impact of long-term warming on BVOC emissions, ecosystem-level
524 emissions are expected to increase in the Arctic due to climate-driven changes in plant biomass
525 and vegetation composition. For instance, the widespread increase in shrub abundance in the Arctic
526 – due to a longer growing season and enhanced nutrient availability (Berner et al., 2018; Sturm et
527 al., 2001) – will likely significantly affect the BVOC emission potential of the Arctic tundra.
528 Additionally, as mentioned above and as discussed extensively by Peñuelas and Staudt (2010) and
529 Loreto and Schnitzler (2010), emissions of BVOCs might be largely beneficial for plants,
530 conferring them higher protection from abiotic stressors which are predicted to be more severe in
531 the future. Long-term arctic warming may thus favor BVOC-emitting species even further.

532 **5. Conclusion**

533 While BVOC ambient concentrations and emission rates have been frequently measured in boreal
534 ecosystems, Arctic tundra environments are under studied. We provide here summertime BVOC
535 ambient air mixing ratios and emission rates at Toolik Field Station, on the north flank of the
536 Brooks Range in northern Alaska. We present the first continuous summertime record of ambient
537 air isoprene and its first-generation oxidation products in the Arctic tundra environment. This
538 dataset provides a new set of observations to constrain isoprene chemistry in low-NO_x
539 environments. This dataset also provides a baseline to investigate future changes in the BVOC
540 emission potential of the Arctic tundra environment. While the overall mean isoprene emission
541 rate amounted to 85 µgC/m²/h, elevated (> 500 µgC/m²/h) isoprene surface emission rates were
542 observed for *Salix* spp., a known isoprene emitter. We also show that the response to temperature
543 of isoprene emissions in enclosures dominated by *Salix* spp. increased exponentially in the 0-40°C
544 range, likely conferring greater thermal protection for these plants. Given the widespread increase
545 in shrub abundance in the Arctic (including *Salix* spp.), our results support earlier studies (e.g.,
546 Valolahti et al., 2015) suggesting that climate-induced changes in the Arctic vegetation
547 composition will significantly affect the BVOC emission potential of the Arctic tundra, with
548 implications for atmospheric oxidation processes and climate feedbacks.

549 **Data availability**

550 Data are available upon request to the corresponding author.

551 **Author contribution**

552 DH, LH, and DBM designed the experiments and acquired funding. HA led the two field
553 campaigns with significant on-site contribution from KM, JH, LH, DBM, KC, JM, CW, TM, and
554 DH. JH designed and built most of the instruments used in this study. CW acquired the PTR-ToF-
555 MS data during the second campaign and DK performed data analysis. MSBH identified the plant
556 species and provided guidance during the field campaigns. KM and HA analyzed the samples in
557 the lab. HA analyzed all the data and prepared the manuscript with contributions from all co-
558 authors.

559 **Competing interests**

560 The authors declare no competing interests.

561 **Acknowledgements**

562 The authors would like to thank CH2MHill Polar Services for logistical support, the Toolik Field
563 Station staff for assistance with the measurements, and Ilann Bourgeois and Georgios Gkatzelis
564 for helpful discussions. The authors also appreciate the help of Anssi Liikanen who offered kind
565 assistance collecting BVOC samples with the tethered balloon and Wade Permar who helped with
566 PTR-ToF-MS measurements. Finally, the authors gratefully acknowledge Claudia Czimczik and
567 Shawn Pedron at the University of California Irvine for letting us use their soil chamber collars.
568 This research was funded by the National Science Foundation grant #1707569. Undergraduate
569 students Katelyn McErlean, Jacob Moss, and Kaixin Cui received financial support from the
570 University of Colorado Boulder's Undergraduate Research Opportunities Program (UROP;
571 reference #5352323, #4422751, and #4332562, respectively).

572 **References**

- 573 Akagi, S. K., Yokelson, R. J., Wiedinmyer, C., Alvarado, M. J., Reid, J. S., Karl, T., Crounse, J.
574 D. and Wennberg, P. O.: Emission factors for open and domestic biomass burning for use in
575 atmospheric models, *Atmospheric Chem. Phys.*, 11(9), 4039–4072,
576 doi:<https://doi.org/10.5194/acp-11-4039-2011>, 2011.
- 577 Apel, E. C., Riemer, D. D., Hills, A., Baugh, W., Orlando, J., Faloona, I., Tan, D., Brune, W.,
578 Lamb, B., Westberg, H., Carroll, M. A., Thornberry, T. and Geron, C. D.: Measurement and
579 interpretation of isoprene fluxes and isoprene, methacrolein, and methyl vinyl ketone mixing ratios
580 at the PROPHET site during the 1998 Intensive, *J. Geophys. Res. Atmospheres*, 107(D3), ACH 7-
581 1-ACH 7-15, doi:10.1029/2000JD000225, 2002.
- 582 Arneth, A., Harrison, S. P., Zaehle, S., Tsigaridis, K., Menon, S., Bartlein, P. J., Feichter, J.,
583 Korhola, A., Kulmala, M., O'Donnell, D., Schurgers, G., Sorvari, S. and Vesala, T.: Terrestrial
584 biogeochemical feedbacks in the climate system, *Nat. Geosci.*, 3(8), 525–532,
585 doi:10.1038/ngeo905, 2010.
- 586 Atkinson, R.: Atmospheric chemistry of VOCs and NO_x, *Atmos. Environ.*, 34(12), 2063–2101,
587 doi:10.1016/S1352-2310(99)00460-4, 2000.
- 588 Bakwin, P. S., Wofsy, S. C., Fan, S.-M. and Fitzjarrald, D. R.: Measurements of NO_x and NO_y
589 concentrations and fluxes over Arctic tundra, *J. Geophys. Res. Atmospheres*, 97(D15), 16545–
590 16557, doi:10.1029/91JD00929, 1992.
- 591 Bates, K. H. and Jacob, D. J.: A new model mechanism for atmospheric oxidation of isoprene:
592 global effects on oxidants, nitrogen oxides, organic products, and secondary organic aerosol,
593 *Atmospheric Chem. Phys.*, 19(14), 9613–9640, doi:<https://doi.org/10.5194/acp-19-9613-2019>,
594 2019.
- 595 Berner, L. T., Jantz, P., Tape, K. D. and Goetz, S. J.: Tundra plant above-ground biomass and
596 shrub dominance mapped across the North Slope of Alaska, *Environ. Res. Lett.*, 13(3), 035002,
597 doi:10.1088/1748-9326/aaaa9a, 2018.
- 598 Biesenthal, T. A. and Shepson, P. B.: Observations of anthropogenic inputs of the isoprene
599 oxidation products methyl vinyl ketone and methacrolein to the atmosphere, *Geophys. Res. Lett.*,
600 24(11), 1375–1378, doi:10.1029/97GL01337, 1997.
- 601 Biesenthal, T. A., Wu, Q., Shepson, P. B., Wiebe, H. A., Anlauf, K. G. and Mackay, G. I.: A study
602 of relationships between isoprene, its oxidation products, and ozone, in the Lower Fraser Valley,
603 BC - ScienceDirect, *Atmospheric Environment*, 31(14), 2049–2058, 1997.
- 604 Carlton, A. G., Wiedinmyer, C. and Kroll, J. H.: A review of Secondary Organic Aerosol (SOA)
605 formation from isoprene, *Atmospheric Chem. Phys.*, 9(14), 4987–5005,
606 doi:<https://doi.org/10.5194/acp-9-4987-2009>, 2009.
- 607 Dobricic, S., Russo, S., Pozzoli, L., Wilson, J. and Vignati, E.: Increasing occurrence of heat waves
608 in the terrestrial Arctic, *Environ. Res. Lett.*, 15(2), 024022, doi:10.1088/1748-9326/ab6398, 2020.

609 Dunne, E., Galbally, I. E., Cheng, M., Selleck, P., Molloy, S. B. and Lawson, S. J.: Comparison
610 of VOC measurements made by PTR-MS, adsorbent tubes–GC-FID-MS and DNPH
611 derivatization–HPLC during the Sydney Particle Study, 2012: a contribution to the assessment of
612 uncertainty in routine atmospheric VOC measurements, *Atmospheric Meas. Tech.*, 11(1), 141–
613 159, doi:<https://doi.org/10.5194/amt-11-141-2018>, 2018.

614 Earth Observatory: Arctic Fires Fill the Skies with Soot, [online] Available from:
615 [https://earthobservatory.nasa.gov/images/145380/arctic-fires-fill-the-skies-with-](https://earthobservatory.nasa.gov/images/145380/arctic-fires-fill-the-skies-with-soot#targetText=In%20June%20and%20July%202019,harmful%20particles%20into%20the%20air)
616 [soot#targetText=In%20June%20and%20July%202019,harmful%20particles%20into%20the%20](https://earthobservatory.nasa.gov/images/145380/arctic-fires-fill-the-skies-with-soot#targetText=In%20June%20and%20July%202019,harmful%20particles%20into%20the%20air)
617 [air.](https://earthobservatory.nasa.gov/images/145380/arctic-fires-fill-the-skies-with-soot#targetText=In%20June%20and%20July%202019,harmful%20particles%20into%20the%20air) (Accessed 16 October 2019), 2019.

618 Ekberg, A., Arneth, A., Hakola, H., Hayward, S. and Holst, T.: Isoprene emission from wetland
619 sedges, *Biogeosciences*, 6(4), 601–613, doi:[10.5194/bg-6-601-2009](https://doi.org/10.5194/bg-6-601-2009), 2009.

620 Ekberg, A., Arneth, A. and Holst, T.: Isoprene emission from Sphagnum species occupying
621 different growth positions above the water table, *Boreal Environ. Res. Int. Interdiscip. J.*, 16(1),
622 47–59, 2011.

623 Elmendorf, S. C., Henry, G. H. R., Hollister, R. D., Björk, R. G., Boulanger-Lapointe, N., Cooper,
624 E. J., Cornelissen, J. H. C., Day, T. A., Dorrepaal, E., Elumeeva, T. G., Gill, M., Gould, W. A.,
625 Harte, J., Hik, D. S., Hofgaard, A., Johnson, D. R., Johnstone, J. F., Jónsdóttir, I. S., Jorgenson, J.
626 C., Klanderud, K., Klein, J. A., Koh, S., Kudo, G., Lara, M., Lévesque, E., Magnússon, B., May,
627 J. L., Mercado-Dí'az, J. A., Michelsen, A., Molau, U., Myers-Smith, I. H., Oberbauer, S. F.,
628 Onipchenko, V. G., Rixen, C., Schmidt, N. M., Shaver, G. R., Spasojevic, M. J., Þórhallsdóttir, Þ.
629 E., Tolvanen, A., Troxler, T., Tweedie, C. E., Villareal, S., Wahren, C.-H., Walker, X., Webber,
630 P. J., Welker, J. M. and Wipf, S.: Plot-scale evidence of tundra vegetation change and links to
631 recent summer warming, *Nat. Clim. Change*, 2(6), 453–457, doi:[10.1038/nclimate1465](https://doi.org/10.1038/nclimate1465), 2012.

632 Faiola, C. L., Erickson, M. H., Fricaud, V. L., Jobson, B. T. and VanReken, T. M.
633 (orcid:0000000226454911): Quantification of biogenic volatile organic compounds with a flame
634 ionization detector using the effective carbon number concept, *Atmospheric Meas. Tech. Online*,
635 5(8), doi:[10.5194/amt-5-1911-2012](https://doi.org/10.5194/amt-5-1911-2012), 2012.

636 Fares, S., Schnitzhofer, R., Jiang, X., Guenther, A., Hansel, A. and Loreto, F.: Observations of
637 Diurnal to Weekly Variations of Monoterpene-Dominated Fluxes of Volatile Organic Compounds
638 from Mediterranean Forests: Implications for Regional Modeling, *Environ. Sci. Technol.*, 47(19),
639 11073–11082, doi:[10.1021/es4022156](https://doi.org/10.1021/es4022156), 2013.

640 Faubert, P., Tiiva, P., Rinnan, Å., Michelsen, A., Holopainen, J. K. and Rinnan, R.: Doubled
641 volatile organic compound emissions from subarctic tundra under simulated climate warming,
642 *New Phytol.*, 187(1), 199–208, doi:[10.1111/j.1469-8137.2010.03270.x](https://doi.org/10.1111/j.1469-8137.2010.03270.x), 2010.

643 Fehsenfeld, F., Calvert, J., Fall, R., Goldan, P., Guenther, A. B., Hewitt, C. N., Lamb, B., Liu, S.,
644 Trainer, M., Westberg, H. and Zimmerman, P.: Emissions of volatile organic compounds from
645 vegetation and the implications for atmospheric chemistry, *Glob. Biogeochem. Cycles*, 6(4), 389–
646 430, doi:[10.1029/92GB02125](https://doi.org/10.1029/92GB02125), 1992.

647 Fontijn, Arthur., Sabadell, A. J. and Ronco, R. J.: Homogeneous chemiluminescent measurement
648 of nitric oxide with ozone. Implications for continuous selective monitoring of gaseous air
649 pollutants, *Anal. Chem.*, 42(6), 575–579, doi:10.1021/ac60288a034, 1970.

650 Forbes, B. C., Fauria, M. M. and Zetterberg, P.: Russian Arctic warming and ‘greening’ are closely
651 tracked by tundra shrub willows, *Glob. Change Biol.*, 16(5), 1542–1554, doi:10.1111/j.1365-
652 2486.2009.02047.x, 2010.

653 Freedman, A. and Cappucci, M.: Parts of Siberia are hotter than Washington, with temperatures
654 nearly 40 degrees above average, *Wash. Post*, 22nd May [online] Available from:
655 <https://www.washingtonpost.com/weather/2020/05/22/siberia-heat-wave/> (Accessed 29 May
656 2020), 2020.

657 Fuentes, J. D., Ler dau, M., Atkinson, R., Baldocchi, D., Bottenheim, J. W., Ciccioli, P., Lamb, B.,
658 Geron, C., Gu, L., Guenther, A., Sharkey, T. D. and Stockwell, W.: Biogenic Hydrocarbons in the
659 Atmospheric Boundary Layer: A Review, *Bull. Am. Meteorol. Soc.*, 81(7), 1537–1576,
660 doi:10.1175/1520-0477(2000)081<1537:BHITAB>2.3.CO;2, 2000.

661 Gough, L.: Relative percent cover of plant species for years 2012-2017 in the Arctic Long-term
662 Ecological Research (ARC-LTER) 1989 moist acidic tundra (MAT89) experimental plots, Toolik
663 Field Station, Alaska., , doi:10.6073/PASTA/F31DEF760DB3F8E6CFEE5FEE07CC693E, 2019.

664 de Gouw, J. A., Goldan, P. D., Warneke, C., Kuster, W. C., Roberts, J. M., Marchewka, M.,
665 Bertman, S. B., Pszenny, A. a. P. and Keene, W. C.: Validation of proton transfer reaction-mass
666 spectrometry (PTR-MS) measurements of gas-phase organic compounds in the atmosphere during
667 the New England Air Quality Study (NEAQS) in 2002, *J. Geophys. Res. Atmospheres*, 108(D21),
668 doi:10.1029/2003JD003863, 2003.

669 Guenther, A., Hewitt, C. N., Erickson, D., Fall, R., Geron, C., Graedel, T., Harley, P., Klinger, L.,
670 Ler dau, M., Mckay, W. A., Pierce, T., Scholes, B., Steinbrecher, R., Tallamraju, R., Taylor, J. and
671 Zimmerman, P.: A global model of natural volatile organic compound emissions, *J. Geophys. Res.*
672 *Atmospheres*, 100(D5), 8873–8892, doi:10.1029/94JD02950, 1995.

673 Guenther, A., Karl, T., Harley, P., Wiedinmyer, C., Palmer, P. I. and Geron, C.: Estimates of global
674 terrestrial isoprene emissions using MEGAN (Model of Emissions of Gases and Aerosols from
675 Nature), *Atmospheric Chem. Phys.*, 6(11), 3181–3210, doi:[https://doi.org/10.5194/acp-6-3181-](https://doi.org/10.5194/acp-6-3181-2006)
676 2006, 2006.

677 Guenther, A. B., Zimmerman, P. R., Harley, P. C., Monson, R. K. and Fall, R.: Isoprene and
678 monoterpene emission rate variability: Model evaluations and sensitivity analyses, *J. Geophys.*
679 *Res. Atmospheres*, 98(D7), 12609–12617, doi:10.1029/93JD00527, 1993.

680 Guenther, A. B., Jiang, X., Heald, C. L., Sakulyanontvittaya, T., Duhl, T., Emmons, L. K. and
681 Wang, X.: The Model of Emissions of Gases and Aerosols from Nature version 2.1 (MEGAN2.1):
682 an extended and updated framework for modeling biogenic emissions, *Geosci. Model Dev.*, 5(6),
683 1471–1492, doi:<https://doi.org/10.5194/gmd-5-1471-2012>, 2012.

684 Hakola, H., Laurila, T., Rinne, J. and Puhto, K.: The ambient concentrations of biogenic
685 hydrocarbons at a northern European, boreal site, *Atmos. Environ.*, 34(29), 4971–4982,
686 doi:10.1016/S1352-2310(00)00192-8, 2000.

687 Hakola, H., Tarvainen, V., Laurila, T., Hiltunen, V., Hellén, H. and Keronen, P.: Seasonal variation
688 of VOC concentrations above a boreal coniferous forest, *Atmos. Environ.*, 37(12), 1623–1634,
689 doi:10.1016/S1352-2310(03)00014-1, 2003.

690 Helmig, D.: Ozone removal techniques in the sampling of atmospheric volatile organic trace gases,
691 *Atmos. Environ.*, 31(21), 3635–3651, doi:10.1016/S1352-2310(97)00144-1, 1997.

692 Helmig, D., Balsley, B., Davis, K., Kuck, L. R., Jensen, M., Bogner, J., Smith, T., Arrieta, R. V.,
693 Rodríguez, R. and Birks, J. W.: Vertical profiling and determination of landscape fluxes of
694 biogenic nonmethane hydrocarbons within the planetary boundary layer in the Peruvian Amazon,
695 *J. Geophys. Res. Atmospheres*, 103(D19), 25519–25532, doi:10.1029/98JD01023, 1998.

696 Helmig, D., Bocquet, F., Pollmann, J. and Reevermann, T.: Analytical techniques for sesquiterpene
697 emission rate studies in vegetation enclosure experiments, *Atmos. Environ.*, 38(4), 557–572,
698 doi:10.1016/j.atmosenv.2003.10.012, 2004.

699 Hollesen, J., Buchwal, A., Rachlewicz, G., Hansen, B. U., Hansen, M. O., Stecher, O. and
700 Elberling, B.: Winter warming as an important co-driver for *Betula nana* growth in western
701 Greenland during the past century, in *Global change biology*, 2015.

702 Holst, T., Arneth, A., Hayward, S., Ekberg, A., Mastepanov, M., Jackowicz-Korczynski, M.,
703 Friberg, T., Crill, P. M. and Bäckstrand, K.: BVOC ecosystem flux measurements at a high latitude
704 wetland site, *Atmospheric Chem. Phys.*, 10(4), 1617–1634, doi:https://doi.org/10.5194/acp-10-
705 1617-2010, 2010.

706 Holton, J. R. and Hakim, G. J.: Chapter 8 - The Planetary Boundary Layer, in *An Introduction to*
707 *Dynamic Meteorology (Fifth Edition)*, edited by J. R. Holton and G. J. Hakim, pp. 255–277,
708 Academic Press, Boston., 2013.

709 Honrath, R. E. and Jaffe, D. A.: The seasonal cycle of nitrogen oxides in the Arctic troposphere at
710 Barrow, Alaska, *J. Geophys. Res. Atmospheres*, 97(D18), 20615–20630, doi:10.1029/92JD02081,
711 1992.

712 Hu, L., Millet, D. B., Baasandorj, M., Griffis, T. J., Turner, P., Helmig, D., Curtis, A. J. and
713 Hueber, J.: Isoprene emissions and impacts over an ecological transition region in the U.S. Upper
714 Midwest inferred from tall tower measurements, *J. Geophys. Res. Atmospheres*, 120(8), 3553–
715 3571, doi:10.1002/2014JD022732, 2015.

716 Isaacman-VanWertz, G., Sueper, D. T., Aikin, K. C., Lerner, B. M., Gilman, J. B., de Gouw, J. A.,
717 Worsnop, D. R. and Goldstein, A. H.: Automated single-ion peak fitting as an efficient approach
718 for analyzing complex chromatographic data, *J. Chromatogr. A*, 1529, 81–92,
719 doi:10.1016/j.chroma.2017.11.005, 2017.

720 Jardine, K. J., Monson, R. K., Abrell, L., Saleska, S. R., Arneth, A., Jardine, A., Ishida, F. Y.,
721 Serrano, A. M. Y., Artaxo, P., Karl, T., Fares, S., Goldstein, A., Loreto, F. and Huxman, T.:
722 Within-plant isoprene oxidation confirmed by direct emissions of oxidation products methyl vinyl
723 ketone and methacrolein, *Glob. Change Biol.*, 18(3), 973–984, doi:10.1111/j.1365-
724 2486.2011.02610.x, 2012.

725 Kade, A., Bret-Harte, M. S., Euskirchen, E. S., Edgar, C. and Fulweber, R. A.: Upscaling of CO₂
726 fluxes from heterogeneous tundra plant communities in Arctic Alaska, *J. Geophys. Res.*
727 *Biogeosciences*, 117(G4), doi:10.1029/2012JG002065, 2012.

728 Karbiwnyk, C. M., Mills, C. S., Helmig, D. and Birks, J. W.: Minimization of water vapor
729 interference in the analysis of non-methane volatile organic compounds by solid adsorbent
730 sampling, *J. Chromatogr. A*, 958(1–2), 219–229, doi:10.1016/s0021-9673(02)00307-2, 2002.

731 Karbiwnyk, C. M., Mills, C. S., Helmig, D. and Birks, J. W.: Use of chlorofluorocarbons as internal
732 standards for the measurement of atmospheric non-methane volatile organic compounds sampled
733 onto solid adsorbent cartridges, *Environ. Sci. Technol.*, 37(5), 1002–1007,
734 doi:10.1021/es025910q, 2003.

735 Karl, T., Potosnak, M., Guenther, A., Clark, D., Walker, J., Herrick, J. D. and Geron, C.: Exchange
736 processes of volatile organic compounds above a tropical rain forest: Implications for modeling
737 tropospheric chemistry above dense vegetation, *J. Geophys. Res. Atmospheres*, 109(D18),
738 doi:10.1029/2004JD004738, 2004.

739 Kramshøj, M., Vedel-Petersen, I., Schollert, M., Rinnan, Å., Nymand, J., Ro-Poulsen, H. and
740 Rinnan, R.: Large increases in Arctic biogenic volatile emissions are a direct effect of warming,
741 *Nat. Geosci.*, 9(5), 349–352, doi:10.1038/ngeo2692, 2016.

742 Kulmala, M., Suni, T., Lehtinen, K. E. J., Maso, M. D., Boy, M., Reissell, A., Rannik, Ü., Aalto,
743 P., Keronen, P., Hakola, H., Bäck, J., Hoffmann, T., Vesala, T. and Hari, P.: A new feedback
744 mechanism linking forests, aerosols, and climate, *Atmospheric Chem. Phys.*, 4(2), 557–562,
745 doi:https://doi.org/10.5194/acp-4-557-2004, 2004.

746 Lader, R., Walsh, J. E., Bhatt, U. S. and Bieniek, P. A.: Projections of Twenty-First-Century
747 Climate Extremes for Alaska via Dynamical Downscaling and Quantile Mapping, *J. Appl.*
748 *Meteorol. Climatol.*, 56(9), 2393–2409, doi:10.1175/JAMC-D-16-0415.1, 2017.

749 Lappalainen, H. K., Sevanto, S., Bäck, J., Ruuskanen, T. M., Kolari, P., Taipale, R., Rinne, J.,
750 Kulmala, M. and Hari, P.: Day-time concentrations of biogenic volatile organic compounds in a
751 boreal forest canopy and their relation to environmental and biological factors, *Atmospheric*
752 *Chem. Phys.*, 9(15), 5447–5459, doi:https://doi.org/10.5194/acp-9-5447-2009, 2009.

753 Li, T., Holst, T., Michelsen, A. and Rinnan, R.: Amplification of plant volatile defence against
754 insect herbivory in a warming Arctic tundra, *Nat. Plants*, 5(6), 568–574, doi:10.1038/s41477-019-
755 0439-3, 2019.

- 756 Lim, H.-J., Carlton, A. G. and Turpin, B. J.: Isoprene Forms Secondary Organic Aerosol through
757 Cloud Processing: Model Simulations, *Environ. Sci. Technol.*, 39(12), 4441–4446,
758 doi:10.1021/es048039h, 2005.
- 759 Lindfors, V., Laurila, T., Hakola, H., Steinbrecher, R. and Rinne, J.: Modeling speciated terpenoid
760 emissions from the European boreal forest, *Atmos. Environ.*, 34(29), 4983–4996,
761 doi:10.1016/S1352-2310(00)00223-5, 2000.
- 762 Lindwall, F., Faubert, P. and Rinnan, R.: Diel Variation of Biogenic Volatile Organic Compound
763 Emissions- A field Study in the Sub, Low and High Arctic on the Effect of Temperature and Light,
764 *PLOS ONE*, 10(4), e0123610, doi:10.1371/journal.pone.0123610, 2015.
- 765 Lindwall, F., Schollert, M., Michelsen, A., Blok, D. and Rinnan, R.: Fourfold higher tundra volatile
766 emissions due to arctic summer warming, *J. Geophys. Res. Biogeosciences*, 121(3), 895–902,
767 doi:10.1002/2015JG003295, 2016.
- 768 Liu, X., Pawliszyn, R., Wang, L. and Pawliszyn, J.: On-site monitoring of biogenic emissions from
769 *Eucalyptus dunnii* leaves using membrane extraction with sorbent interface combined with a
770 portable gas chromatograph system, *The Analyst*, 129(1), 55–62, doi:10.1039/b311998j, 2004.
- 771 Loreto, F. and Schnitzler, J.-P.: Abiotic stresses and induced BVOCs, *Trends Plant Sci.*, 15(3),
772 154–166, doi:10.1016/j.tplants.2009.12.006, 2010.
- 773 Macias-Fauria, M., Forbes, B. C., Zetterberg, P. and Kumpula, T.: Eurasian Arctic greening
774 reveals teleconnections and the potential for structurally novel ecosystems, *Nat. Clim. Change*,
775 2(8), 613–618, doi:10.1038/nclimate1558, 2012.
- 776 Markon, C. J., Trainor, S. F. and Chapin, F. S.: The United States National Climate Assessment -
777 Alaska Technical Regional Report. [online] Available from:
778 <https://pubs.usgs.gov/circ/1379/pdf/circ1379.pdf>, 2012.
- 779 Michelsen, A., Rinnan, R. and Jonasson, S.: Two decades of experimental manipulations of heaths
780 and forest understory in the subarctic, *Ambio*, 41 Suppl 3, 218–230, doi:10.1007/s13280-012-
781 0303-4, 2012.
- 782 Millet, D. B., Alwe, H. D., Chen, X., Deventer, M. J., Griffis, T. J., Holzinger, R., Bertman, S. B.,
783 Rickly, P. S., Stevens, P. S., Léonardis, T., Locoge, N., Dusanter, S., Tyndall, G. S., Alvarez, S.
784 L., Erickson, M. H. and Flynn, J. H.: Bidirectional Ecosystem–Atmosphere Fluxes of Volatile
785 Organic Compounds Across the Mass Spectrum: How Many Matter?, *ACS Earth Space Chem.*,
786 doi:10.1021/acsearthspacechem.8b00061, 2018.
- 787 Olofsson, M., Ek-Olausson, B., Jensen, N. O., Langer, S. and Ljungström, E.: The flux of isoprene
788 from a willow coppice plantation and the effect on local air quality, *Atmos. Environ.*, 39(11),
789 2061–2070, doi:10.1016/j.atmosenv.2004.12.015, 2005.
- 790 Ormeño, E., Mevy, J. P., Vila, B., Bousquet-Melou, A., Greff, S., Bonin, G. and Fernandez, C.:
791 Water deficit stress induces different monoterpene and sesquiterpene emission changes in

- 792 Mediterranean species. Relationship between terpene emissions and plant water potential,
793 *Chemosphere*, 67(2), 276–284, 2007.
- 794 Ortega, J. and Helmig, D.: Approaches for quantifying reactive and low-volatility biogenic organic
795 compound emissions by vegetation enclosure techniques – Part A, *Chemosphere*, 72(3), 343–364,
796 doi:10.1016/j.chemosphere.2007.11.020, 2008.
- 797 Ortega, J., Helmig, D., Daly, R. W., Tanner, D. M., Guenther, A. B. and Herrick, J. D.: Approaches
798 for quantifying reactive and low-volatility biogenic organic compound emissions by vegetation
799 enclosure techniques – Part B: Applications, *Chemosphere*, 72(3), 365–380,
800 doi:10.1016/j.chemosphere.2008.02.054, 2008.
- 801 Overland, J. E., Wang, M., Walsh, J. E. and Stroeve, J. C.: Future Arctic climate changes:
802 Adaptation and mitigation time scales, *Earths Future*, 2(2), 68–74, doi:10.1002/2013EF000162,
803 2014.
- 804 Peñuelas, J. and Staudt, M.: BVOCs and global change, *Trends Plant Sci.*, 15(3), 133–144,
805 doi:10.1016/j.tplants.2009.12.005, 2010.
- 806 Pollmann, J., Ortega, J. and Helmig, D.: Analysis of Atmospheric Sesquiterpenes: Sampling
807 Losses and Mitigation of Ozone Interferences, *Environ. Sci. Technol.*, 39(24), 9620–9629,
808 doi:10.1021/es050440w, 2005.
- 809 Potosnak, M. J., Baker, B. M., LeSturgeon, L., Disher, S. M., Griffin, K. L., Bret-Harte, M. S.
810 and Starr, G.: Isoprene emissions from a tundra ecosystem, *Biogeosciences*, 10(2), 871–889,
811 doi:10.5194/bg-10-871-2013, 2013.
- 812 Pressley, S., Lamb, B., Westberg, H., Flaherty, J., Chen, J. and Vogel, C.: Long-term isoprene flux
813 measurements above a northern hardwood forest, *J. Geophys. Res. Atmospheres*, 110(D7),
814 doi:10.1029/2004JD005523, 2005.
- 815 Reynolds, M. K., Walker, D. A., Balsler, A., Bay, C., Campbell, M., Cherosov, M. M., Daniëls, F.
816 J. A., Eidesen, P. B., Ermokhina, K. A., Frost, G. V., Jdrzejek, B., Jorgenson, M. T., Kennedy,
817 B. E., Kholod, S. S., Lavrinenko, I. A., Lavrinenko, O. V., Magnússon, B., Matveyeva, N. V.,
818 Metúsalemsson, S., Nilsen, L., Olthof, I., Pospelov, I. N., Pospelova, E. B., Pouliot, D., Razzhivin,
819 V., Schaepman-Strub, G., Šibík, J., Telyatnikov, M. Yu. and Troeva, E.: A raster version of the
820 Circumpolar Arctic Vegetation Map (CAVM), *Remote Sens. Environ.*, 232, 111297,
821 doi:10.1016/j.rse.2019.111297, 2019.
- 822 Rinnan, R., Rinnan, Å., Faubert, P., Tiiva, P., Holopainen, J. K. and Michelsen, A.: Few long-term
823 effects of simulated climate change on volatile organic compound emissions and leaf chemistry of
824 three subarctic dwarf shrubs, *Environ. Exp. Bot.*, 72(3), 377–386,
825 doi:10.1016/j.envexpbot.2010.11.006, 2011.
- 826 Rinnan, R., Steinke, M., McGenity, T. and Loreto, F.: Plant volatiles in extreme terrestrial and
827 marine environments, *Plant Cell Environ.*, 37(8), 1776–1789, doi:10.1111/pce.12320, 2014.

- 828 Rinne, H. J. I., Guenther, A. B., Greenberg, J. P. and Harley, P. C.: Isoprene and monoterpene
829 fluxes measured above Amazonian rainforest and their dependence on light and temperature,
830 *Atmos. Environ.*, 36(14), 2421–2426, doi:10.1016/S1352-2310(01)00523-4, 2002.
- 831 Rinne, J., Bäck, J. and Hakola, H.: Biogenic volatile organic compound emissions from the
832 Eurasian taiga: current knowledge and future directions, , 14, 20, 2009.
- 833 Rivera-Rios, J. C., Nguyen, T. B., Crouse, J. D., Jud, W., Clair, J. M. S., Mikoviny, T., Gilman,
834 J. B., Lerner, B. M., Kaiser, J. B., Gouw, J. de, Wisthaler, A., Hansel, A., Wennberg, P. O.,
835 Seinfeld, J. H. and Keutsch, F. N.: Conversion of hydroperoxides to carbonyls in field and
836 laboratory instrumentation: Observational bias in diagnosing pristine versus anthropogenically
837 controlled atmospheric chemistry, *Geophys. Res. Lett.*, 41(23), 8645–8651,
838 doi:10.1002/2014GL061919, 2014.
- 839 Ruuskanen, T. M., Kolari, P., Bäck, J., Kulmala, M., Rinne, J., Hakola, H., Taipale, R., Raivonen,
840 M., Altimir, N. and Hari, P.: On-line field measurements of monoterpene emissions from Scots
841 pine by proton-transfer-reaction mass spectrometry, *Boreal Environ. Res.*, 10(6), 553–567, 2005.
- 842 Sasaki, K., Saito, T. and Lamsa, M.: Plants utilize isoprene emission as a thermotolerance
843 mechanism, *Plant Cell Physiol.*, 48, 1254–1262, 2007.
- 844 Scanlon, J. T. and Willis, D. E.: Calculation of Flame Ionization Detector Relative Response
845 Factors Using the Effective Carbon Number Concept, *J. Chromatogr. Sci.*, 23(8), 333–340,
846 doi:10.1093/chromsci/23.8.333, 1985.
- 847 Schollert, M., Burchard, S., Faubert, P., Michelsen, A. and Rinnan, R.: Biogenic volatile organic
848 compound emissions in four vegetation types in high arctic Greenland, *Polar Biol.*, 37(2), 237–
849 249, doi:10.1007/s00300-013-1427-0, 2014.
- 850 Schollert, M., Kivimäenpää, M., Valolahti, H. M. and Rinnan, R.: Climate change alters leaf
851 anatomy, but has no effects on volatile emissions from arctic plants, *Plant Cell Environ.*, 38(10),
852 2048–2060, doi:10.1111/pce.12530, 2015.
- 853 Shaver, G. R. and Chapin, F. S.: Production: Biomass Relationships and Element Cycling in
854 Contrasting Arctic Vegetation Types, *Ecol. Monogr.*, 61(1), 1–31, doi:10.2307/1942997, 1991.
- 855 Sindelarova, K., Granier, C., Bouarar, I., Guenther, A., Tilmes, S., Stavrakou, T., Müller, J.-F.,
856 Kuhn, U., Stefani, P. and Knorr, W.: Global data set of biogenic VOC emissions calculated by the
857 MEGAN model over the last 30 years, *Atmospheric Chem. Phys.*, 14(17), 9317–9341,
858 doi:https://doi.org/10.5194/acp-14-9317-2014, 2014.
- 859 Sistla, S. A., Moore, J. C., Simpson, R. T., Gough, L., Shaver, G. R. and Schimel, J. P.: Long-term
860 warming restructures Arctic tundra without changing net soil carbon storage, *Nature*, 497(7451),
861 615–618, doi:10.1038/nature12129, 2013.
- 862 Spirig, C., Guenther, A., Greenberg, J. P., Calanca, P. and Tarvainen, V.: Tethered balloon
863 measurements of biogenic volatile organic compounds at a Boreal forest site, *Atmospheric Chem.*
864 *Phys.*, 4(1), 215–229, doi:https://doi.org/10.5194/acp-4-215-2004, 2004.

- 865 Sturm, M., Racine, C. and Tape, K.: Climate change: Increasing shrub abundance in the Arctic,
866 *Nature*, 411(6837), 546–547, doi:10.1038/35079180, 2001.
- 867 Sullivan, P. F., Sommerkorn, M., Rueth, H. M., Nadelhoffer, K. J., Shaver, G. R. and Welker, J.
868 M.: Climate and species affect fine root production with long-term fertilization in acidic tussock
869 tundra near Toolik Lake, Alaska, *Oecologia*, 153(3), 643–652, doi:10.1007/s00442-007-0753-8,
870 2007.
- 871 Survey: Maps - Toolik Lake Area Vegetation, [online] Available from:
872 <http://www.arcticatlas.org/maps/themes/tl5k/tl5kvg> (Accessed 30 September 2019), 2012.
- 873 Tang, J., Schurgers, G., Valolahti, H., Faubert, P., Tiiva, P., Michelsen, A. and Rinnan, R.:
874 Challenges in modelling isoprene and monoterpene emission dynamics of Arctic plants: a case
875 study from a subarctic tundra heath, *Biogeosciences*, 13(24), 6651–6667,
876 doi:<https://doi.org/10.5194/bg-13-6651-2016>, 2016.
- 877 Tape, K., Sturm, M. and Racine, C.: The evidence for shrub expansion in Northern Alaska and the
878 Pan-Arctic, *Glob. Change Biol.*, 12(4), 686–702, doi:10.1111/j.1365-2486.2006.01128.x, 2006.
- 879 Tarvainen, V., Hakola, H., Rinne, J., HelläN, H. and Haapanala, S.: Towards a comprehensive
880 emission inventory of terpenoids from boreal ecosystems, *Tellus B Chem. Phys. Meteorol.*, 59(3),
881 526–534, doi:10.1111/j.1600-0889.2007.00263a.x, 2007.
- 882 Tiiva, P., Faubert, P., Michelsen, A., Holopainen, T., Holopainen, J. K. and Rinnan, R.: Climatic
883 warming increases isoprene emission from a subarctic heath, *New Phytol.*, 180(4), 853–863,
884 doi:10.1111/j.1469-8137.2008.02587.x, 2008.
- 885 Toolik Field Station Environmental Data Center: Toolik Field Station::Weather Data Query,
886 [online] Available from: https://toolik.alaska.edu/edc/abiotic_monitoring/data_query.php
887 (Accessed 30 September 2019), 2019.
- 888 Tsigaridis, K. and Kanakidou, M.: Secondary organic aerosol importance in the future atmosphere,
889 *Atmos. Environ.*, 41(22), 4682–4692, doi:10.1016/j.atmosenv.2007.03.045, 2007.
- 890 Unger, N.: Human land-use-driven reduction of forest volatiles cools global climate, *Nat. Clim.*
891 *Change*, 4(10), 907–910, doi:10.1038/nclimate2347, 2014.
- 892 Valolahti, H., Kivimäenpää, M., Faubert, P., Michelsen, A. and Rinnan, R.: Climate change-
893 induced vegetation change as a driver of increased subarctic biogenic volatile organic compound
894 emissions, *Glob. Change Biol.*, 21(9), 3478–3488, doi:10.1111/gcb.12953, 2015.
- 895 Van Dam, B., Helmig, D., Burkhart, J. F., Obrist, D. and Oltmans, S. J.: Springtime boundary layer
896 O₃ and GEM depletion at Toolik Lake, Alaska, *J. Geophys. Res. Atmospheres*, 118(8), 3382–
897 3391, doi:10.1002/jgrd.50213, 2013.
- 898 Van Dam, B., Helmig, D., Doskey, P. V. and Oltmans, S. J.: Summertime surface O₃ behavior
899 and deposition to tundra in the Alaskan Arctic, *J. Geophys. Res. Atmospheres*, 121(13), 8055–
900 8066, doi:10.1002/2015JD023914, 2016.

- 901 Vedel-Petersen, I., Schollert, M., Nymand, J. and Rinnan, R.: Volatile organic compound emission
902 profiles of four common arctic plants, *Atmos. Environ.*, 120, 117–126,
903 doi:10.1016/j.atmosenv.2015.08.082, 2015.
- 904 Walker, M. D., Walker, D. A. and Auerbach, N. A.: Plant communities of a tussock tundra
905 landscape in the Brooks Range Foothills, Alaska, *J. Veg. Sci.*, 5(6), 843–866,
906 doi:10.2307/3236198, 1994.
- 907 Wang, J.-L., Chew, C., Chen, S.-W. and Kuo, S.-R.: Concentration Variability of Anthropogenic
908 Halocarbons and Applications as Internal Reference in Volatile Organic Compound
909 Measurements, *Environ. Sci. Technol.*, 34(11), 2243–2248, doi:10.1021/es991128n, 2000.
- 910 Zini, C. A., Augusto, F., Christensen, T. E., Smith, B. P., Caramão, E. B. and Pawliszy, J.:
911 Monitoring biogenic volatile compounds emitted by *Eucalyptus citriodora* using SPME, *Anal.*
912 *Chem.*, 73(19), 4729–4735, doi:10.1021/ac0103219, 2001.
- 913

914 Table 1: Year 2017 median relative percent cover of plant species in moist acidic tundra long-term
 915 ecological research (LTER) experimental control plots at Toolik Field Station. The last column indicates
 916 whether plant species were present in surface or bag enclosure experiments in this study.

Plant name	Relative land surface cover in moist acidic tundra (%) (Gough, 2019)	Present in surface or bag enclosures
<i>Andromeda polifolia</i>	0.6	yes
<i>Betula nana</i>	14.4	yes
<i>Carex bigelowii</i>	1.0	yes
<i>Cassiope tetragona</i>	2.0	yes
<i>Empetrum nigrum</i>	3.8	yes
<i>Eriophorum vaginatum</i>	8.6	yes
<i>Ledum palustre</i>	10.5	yes
<i>Mixed Lichens</i>	2.1	yes
<i>Mixed moss</i>	6.0	yes
<i>Pedicularis lapponica</i>	0.6	no
<i>Polygonum bistorta</i>	0.6	no
<i>Rubus chamaemorus</i>	20.2	no
<i>Salix pulchra</i>	4.9	yes
<i>Vaccinium uliginosum</i>	1.9	yes
<i>Vaccinium vitis-idaea</i>	6.6	yes

917
 918
 919
 920
 921

922 Table 2: Average mixings ratios with standard deviation, along with minimum (min) and maximum (max)
 923 values and quantification frequency (QF) of the measured monoterpenes in ambient air. LOQ stands for
 924 limit of quantification. For values lower than the LOQ, mixing ratios equal to half of the LOQ were used
 925 to calculate the mean.

	mean \pm standard deviation (pptv)	Min (pptv)	Max (pptv)	QF (%)
α -pinene	11.7 \pm 8.1	< LOQ	61.6	88
camphene	< LOQ	< LOQ	21.9	11
sabinene	< LOQ	< LOQ	34.2	11
p-cymene	2.0 \pm 1.9	< LOQ	12.3	32
limonene	< LOQ	< LOQ	2.9	< 1

926

927

928

929

930

931

932

933

934

935

936

937

938

939

940 Table 3: Isoprene and monoterpenes (sum of α -pinene, β -pinene, limonene, and 1,8-cineole) surface
 941 emission rates per vegetation type. Miscellaneous refers to a mix of different species, including lichens and
 942 moss tundra (see Fig.S.I.3-15). Daytime refers to 10 am-8 pm, midday to 11 am-2 pm, and nighttime to 11
 943 pm-5 am (Alaska Standard Time). The values in brackets represent the average enclosure temperature for
 944 each emission rate.

	mean \pm standard deviation ($\mu\text{gC}/\text{m}^2/\text{h}$)	daytime mean \pm standard deviation ($\mu\text{gC}/\text{m}^2/\text{h}$)	midday mean \pm standard deviation ($\mu\text{gC}/\text{m}^2/\text{h}$)	nighttime mean \pm standard deviation ($\mu\text{gC}/\text{m}^2/\text{h}$)
isoprene				
<i>Salix</i> spp.	149 \pm 327 [17.6°C]	232 \pm 400 [23.9°C]	334 \pm 473 [27.0°C]	7 \pm 10 [8.0°C]
<i>Betula</i> spp.	12 \pm 30 [13.7°C]	19 \pm 38 [17.4°C]	28 \pm 37 [20.1°C]	5 \pm 14 [5.8°C]
Miscellaneous	38 \pm 81 [11.8°C]	57 \pm 100 [14.8°C]	104 \pm 135 [16.2°C]	21 \pm 64 [8.2°C]
monoterpenes				
<i>Salix</i> spp.	0.8 \pm 1.3 [17.6°C]	1.1 \pm 1.5 [23.9°C]	1.4 \pm 1.7 [27.0°C]	0.4 \pm 1.0 [8.0°C]
<i>Betula</i> spp.	0.5 \pm 0.6 [13.7°C]	0.7 \pm 0.7 [17.4°C]	1.0 \pm 0.8 [20.1°C]	0.2 \pm 0.2 [5.8°C]
Miscellaneous	1.1 \pm 1.4 [11.8°C]	1.3 \pm 1.6 [14.8°C]	1.7 \pm 2.0 [16.2°C]	1.0 \pm 1.4 [8.2°C]

945

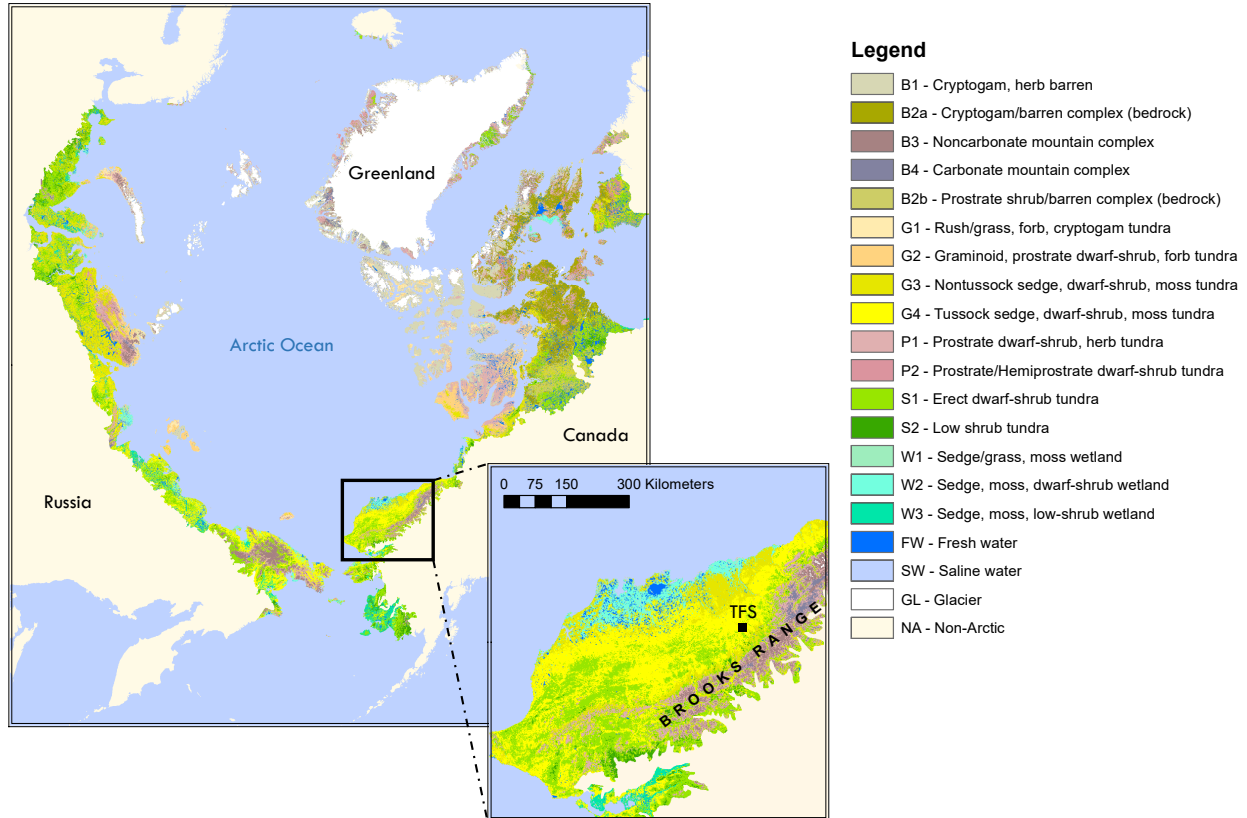
946

947

948

949

950



951

952 Figure 1: Location of Toolik Field Station (TFS) on the north flanks of the Brooks Range in northern Alaska
 953 along with arctic vegetation type. This Figure was made using the raster version of the Circumpolar Arctic
 954 Vegetation Map prepared by Reynolds et al. (2019) and publicly available at www.geobotany.uaf.edu.

955

956

957

958

959

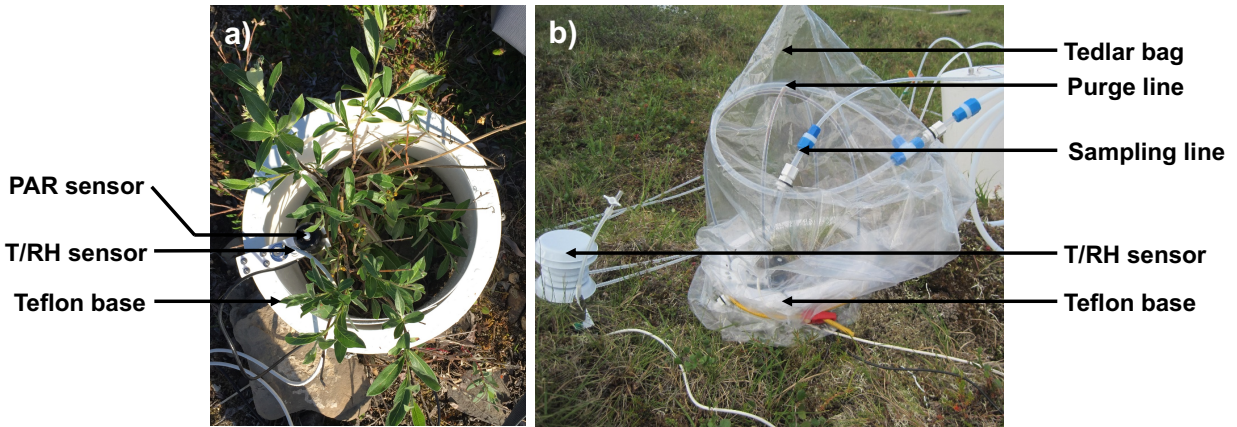
960

961

962

963

964



965

966 Figure 2: Photographs of a surface enclosure experiment setup at Toolik Field Station, Alaska. a) The first
 967 step of the installation consisted in positioning the Teflon® base around the vegetation of interest along
 968 with temperature (T), relative humidity (RH), and photosynthetically active radiation (PAR) sensors. b)
 969 The second step consisted in positioning the Tedlar® bag around the base. The bag was connected to a
 970 purge air and a sampling line. An additional T/RH sensor was also positioned outside the bag.

971

972

973

974

975

976

977

978

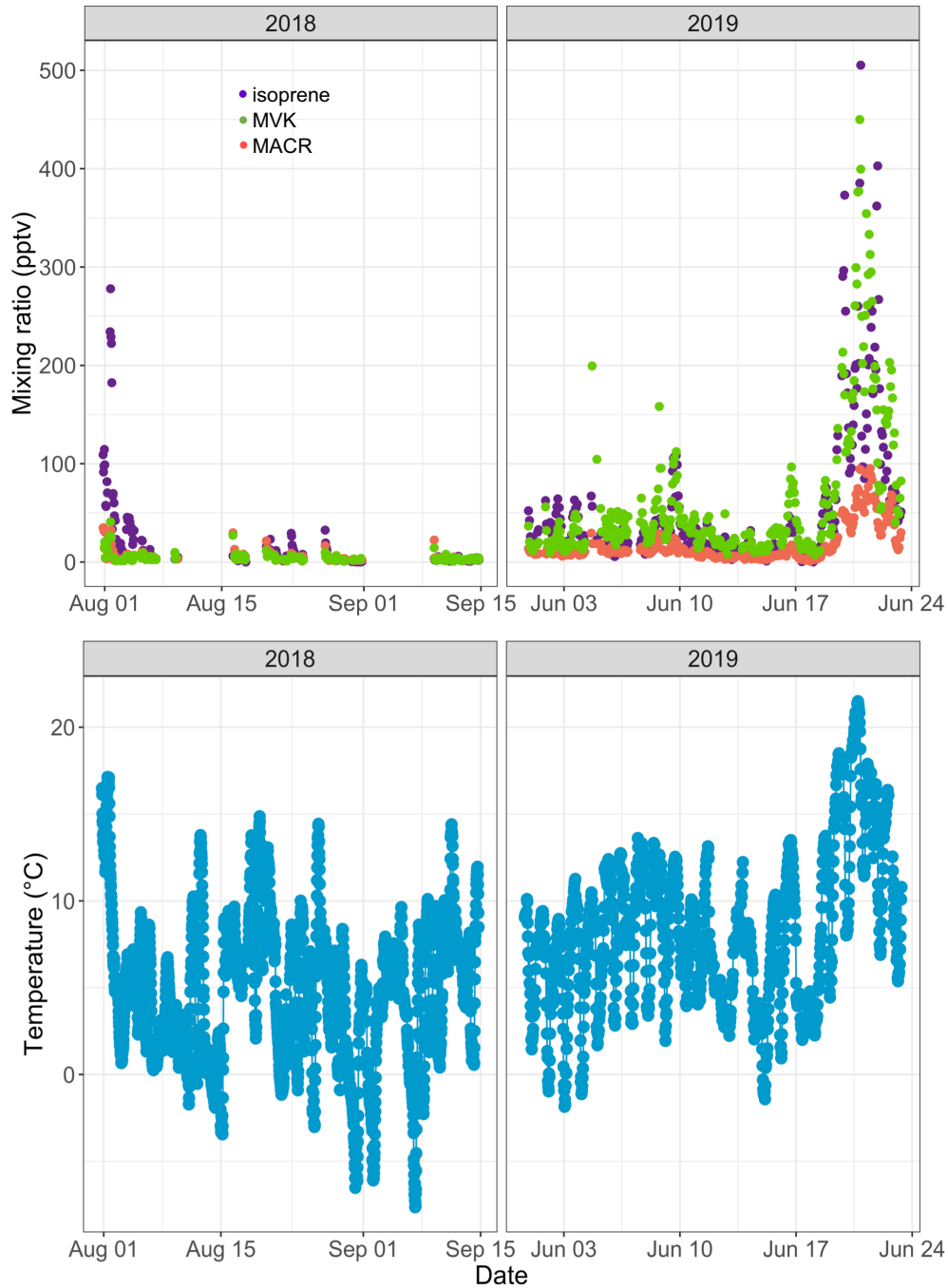
979

980

981

982

983

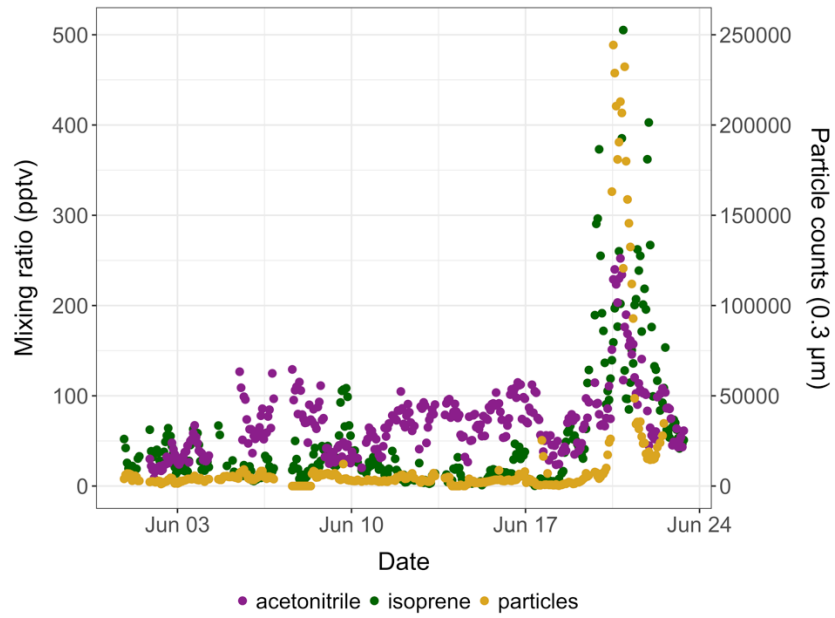


984

985 Figure 3: Time-series of isoprene (purple), methylvinylketone (MVK, green), and methacrolein (MACR,
 986 salmon) mixing ratios (in pptv) in ambient air at Toolik Field station (top panels) and of 30-min-averaged
 987 ambient temperature (in °C) at 4 meters above ground level (bottom panels).

988

989



990

991 Figure 4: Time-series of isoprene (green) and acetonitrile (purple) mixing ratios (in pptv) and of 0.3 μm
 992 particle counts (yellow) in ambient air at Toolik Field station in June 2019.

993

994

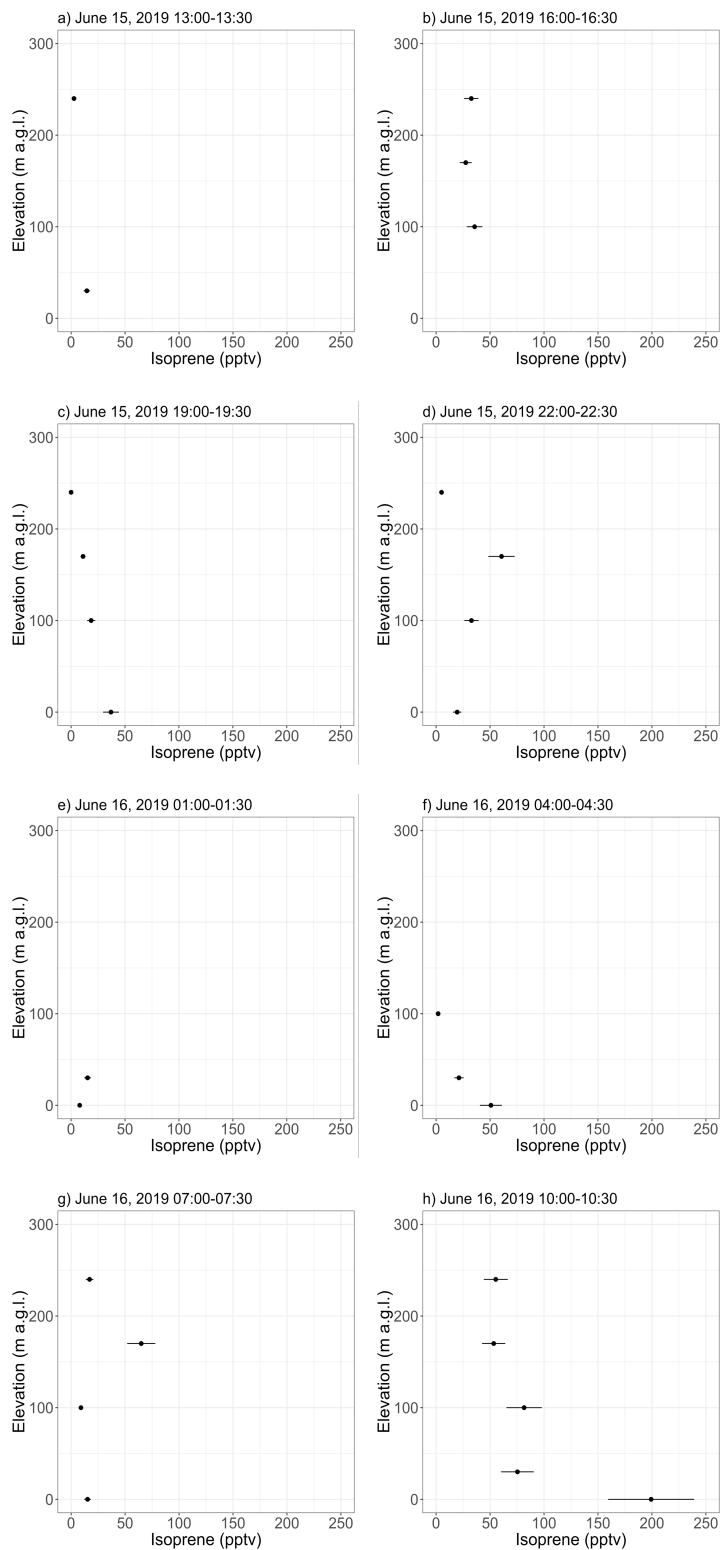
995

996

997

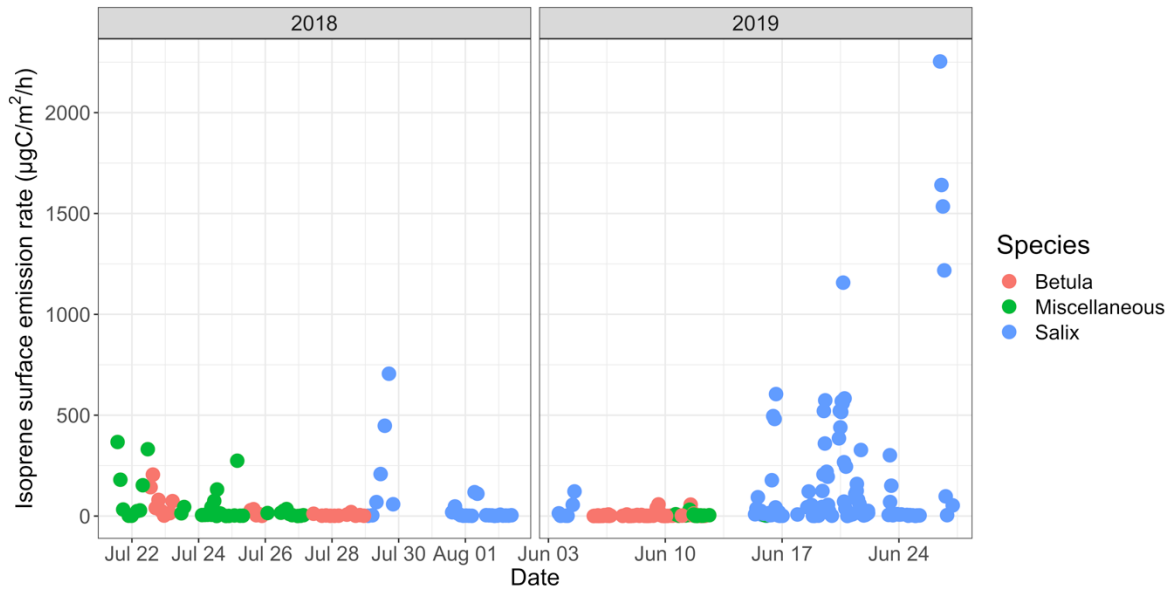
998

999



1000

1001 Figure 5: Vertical profiles of isoprene mixing ratios as inferred from 30-min samples collected with a
 1002 tethered balloon. The error bars show the analytical uncertainty for isoprene (20 %). Samples with an
 1003 isoprene mixing ratio lower than blanks were discarded. Hours are in Alaska Standard Time (UTC-9).



1004

1005 Figure 6: Time-series of isoprene surface emission rates (in $\mu\text{gC}/\text{m}^2/\text{h}$) for different vegetation types.

1006 Miscellaneous refers to a mix of different species, including lichens and moss tundra.

1007

1008

1009

1010

1011

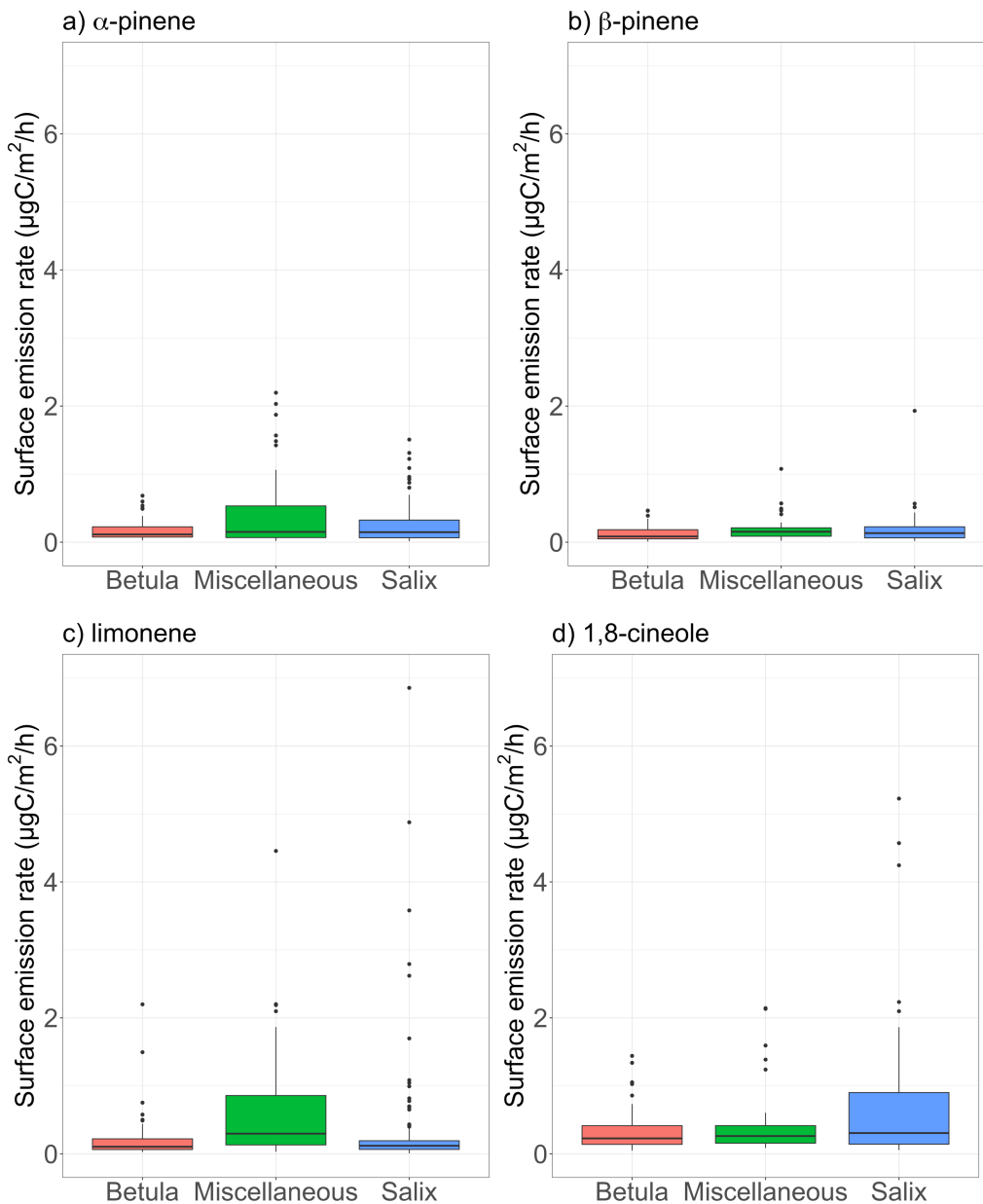
1012

1013

1014

1015

1016

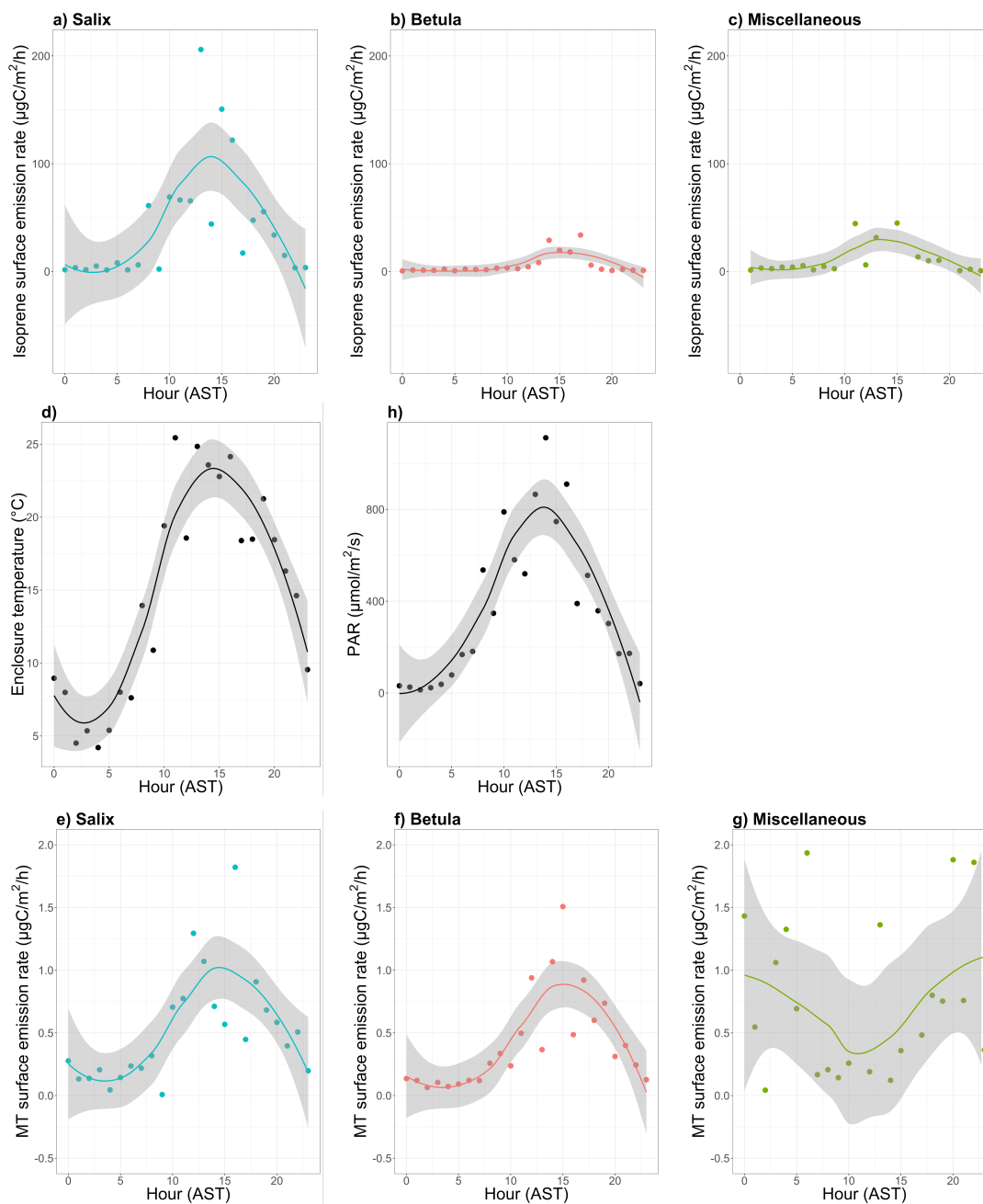


1017

1018 Figure 7: Surface emission rates of various monoterpenes (in $\mu\text{gC}/\text{m}^2/\text{h}$) for different vegetation types. The
 1019 lower and upper hinges correspond to the first and third quartiles. The upper (lower) whisker extends from
 1020 the hinge to the largest (smallest) value no further than $1.5 \times IQR$ from the hinge, where IQR is the inter-
 1021 quartile range (i.e., the distance between the first and third quartiles). The notches extend $1.58 \times IQR/\sqrt{n}$
 1022 and give a $\sim 95\%$ confidence interval for medians. Miscellaneous refers to a mix of different species,
 1023 including lichens and moss tundra.

1024

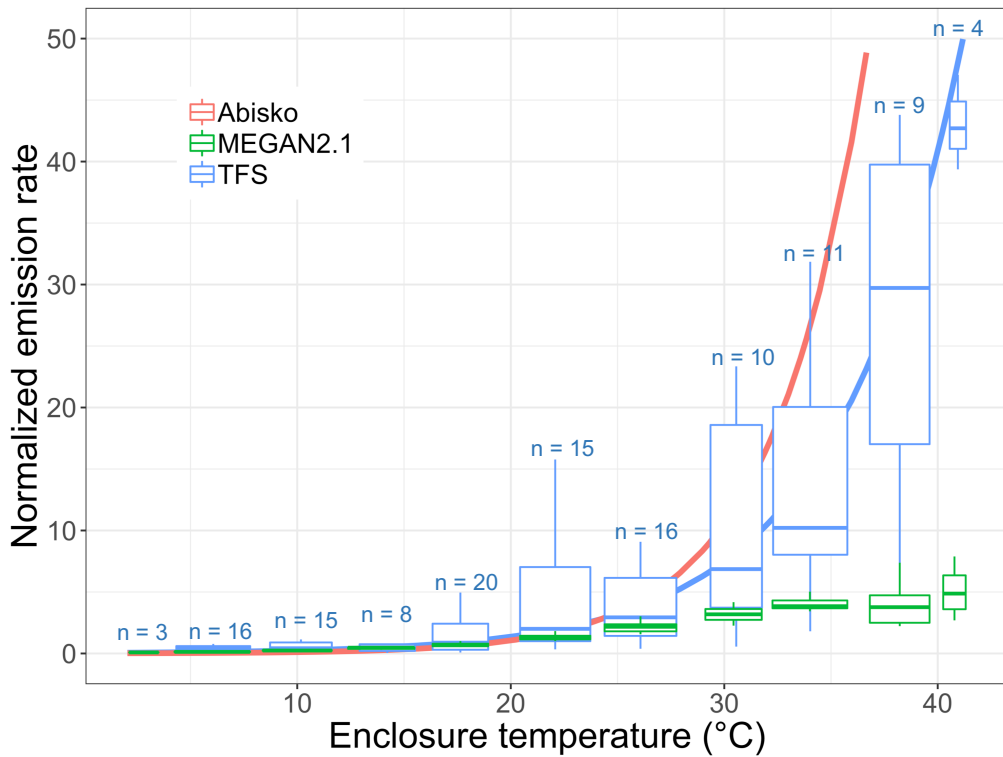
1025



1026

1027 Figure 8: Mean diurnal cycle of isoprene (a-c) and monoterpenes (MT; e-g) surface emission rates (in
 1028 $\mu\text{gC}/\text{m}^2/\text{h}$ – note the difference scale on the y-axis), d) enclosure temperature (in $^{\circ}\text{C}$), and h) enclosure
 1029 photosynthetically active radiation (PAR in $\mu\text{mol}/\text{m}^2/\text{s}$). The dots represent the hourly means. The line is
 1030 the smoothed conditional mean while the grey shaded region indicates the 95% confidence interval. Hours
 1031 are in Alaska Standard Time (UTC-9) and correspond to the end of the 2-hr sampling period for isoprene
 1032 and MT emission rates. MT corresponds here to the sum of α -pinene, β -pinene, limonene, and 1,8-cineole.
 1033 Miscellaneous refers to a mix of different species, including lichens and moss tundra.

1034



1035

1036 Figure 9: Normalized isoprene surface emission rate (emissions at 20°C set equal to 1.0) as a function of
1037 enclosure temperature (in °C). This figure shows the response to temperature as observed at Toolik Field
1038 Station (TFS, in blue) and Abisko, Sweden (in pink; Tang et al., 2016), and as parameterized in MEGAN2.1
1039 (in green). The blue solid line is the exponential fit at TFS. n denotes the number of measurements in each
1040 enclosure temperature bin. It should be noted that the enclosure temperature was on average 5-6°C warmer
1041 than ambient air due to greenhouse heating.